DOE/PC/9005-T34

LIQUID PHASE METHANOL LAPORTE PROCESS DEVELOPMENT UNIT: RESEARCH AND ENGINEERING SUPPORT STUDIES

Topical Report

Task 3.4: Adsorbent Evaluation for Removal of Catalyst Poisons From Synthesis Gas

Contractor

AIR PRODUCTS AND CHEMICALS, INC.
Allentown, PA 18195

And

Subcontractor to Air Products

CHEM SYSTEMS INC.
Tarrytown, NY 10591

28 September 1990

Prepared for the United States Department of Energy
Under Contract No. DE-AC22-87PC90005
Contract Period 9 April 1987 – 9 October 1990

0551J-IA

DISCLAIMER

Abstract

Operation of a methanol synthesis reactor in the liquid phase requires an efficient catalyst poison removal system. A number of commercially available adsorbents were screened for their ability to remove the following methanol catalyst poisons: $Fe(CO)_5$, $Ni(CO)_4$, COS, H_2S, and HCl. Adsorption isotherms were measured at various carrier gas pressures and two temperatures on several adsorbents, including active carbons, zeolites, alumina, silica gel, metal oxide impregnated active carbons, metal oxide promoted zinc oxide, metal oxide promoted alumina, and spent methanol catalyst. By monitoring the approach to equilibrium as a function of time, mass transfer coefficients for the adsorption of these trace impurities were also determined. From this adsorbent screening, the preferred adsorbent for removal of each catalyst poison was identified. The equilibrium and kinetic adsorptive properties for each poison/adsorbent system were used to design a poison removal scheme. This design will be tested in a pilot unit using coal gas from a commercial gasifier.

Table of Contents

List of Tables

List of Figures

List of Figures
(continued)

INTRODUCTION

Traditionally, catalytic conversion of synthesis gas (mixtures of CO and H_2) to chemicals or fuels is carried out in a fixed bed reactor. In 1975, Chem Systems Inc. began to investigate the possibility of producing methanol from synthesis gas in a liquid phase reactor (1). Air Products began research to further develop this technology in 1981. In this scheme, the catalyst is suspended in an inert liquid, typically a hydrocarbon oil. The reactor may be designed as an ebullated bed using a particulate catalyst, or may be designed as a slurry reactor with a catalyst powder. In either case, the synthesis gas bubbles up through the reactor and is converted to methanol. The methanol leaves the reactor as a vapor with the unreacted gas. Because of the large heat sink provided by the liquid phase process, heat removal is greatly facilitated and reactor temperature control is quite straightforward. The catalyst zone is essentially isothermal, and an operating temperature can be selected that is low enough to avoid the equilibrium constraints of gas phase reactors, yet high enough to produce a substantial rate of reaction. Since temperature rise is less of a constraint, it is possible to achieve a high conversion of synthesis gas to methanol on each pass through the reactor as well as reduce catalyst deactivation rates.

However, the liquid phase reaction does have a disadvantage. Synthesis gas produced from coal gasification contains a number of impurities which can deactivate the methanol catalyst. In the standard fixed bed reactor, the front end of the catalyst bed acts as a poisons removal system. On the other

hand, in a slurry reactor, the catalyst poisons are spread throughout the system and not restricted to the feed end as in the fixed bed case. Hence, efficient catalyst poison removal is an essential aspect of the liquid phase methanol process.

Due to the importance of catalyst poison removal in the liquid phase reactor design, the current investigation was initiated. Table 1 shows typical impurities and their concentrations in synthesis gas generated from coal gasification. This investigation involved measuring both the equilibrium and kinetic adsorptive characteristics of various commercial adsorbents for a variety of methanol catalyst poisons including $Fe(CO)_5$, $Ni(CO)_4$, H_2S, COS, and HCl. From these data, a catalyst removal system was designed. This design was tested at the pilot unit scale with actual coal gasifier off-gas.

OBJECTIVE:

The objective of this investigation was to gather adsorption data on the trace removal of methanol catalyst poisons $Fe(CO)_5$, $Ni(CO)_4$, H_2S, COS, and HCl using various commercial adsorbents. This data was then used to design a catalyst poison removal system which was tested with actual coal gasifier off-gas. The pertinent data needed to design such a system include 1) the equilibrium capacity of the chosen adsorbent for the given trace impurity and the shape of the adsorption isotherm, 2) the length of the mass transfer zone (MTZ) required for the removal of the trace compound, 3) the interactions that exist between individual trace compounds and the carrier gas which effect adsorption equilibrium and MTZ lengths, and 4) the ease and effect of regeneration on the spent adsorbents.

TABLE 1
MAJOR TRACE CONTAMINANTS IN LPMEOH SYNGAS FEED

Trace Component	Design Concentration, ppmv: Adsorber Feed Limit	Design Concentration, ppmv: Catalyst Design Limit	Turbine Fuel Gas Specs., ppmv
Sulfur Compounds*			
H_2S	5		
COS	10		
Total Sulfur	15	0.06	
Halides			
Chloride	20		<10
Fluoride	5		
Total Halides		0.01	
Hydrocarbons			
Ethylene, Benzene and Other Unsaturates	2	300	
Acetylene	1	5.0	
Nitrogen Compounds			
NH_3	5	10.0	
NO_x	0.001	0.1	
HCN	6	0.01	
Oxygen		1500	
Water	0-1500		
Selexol (polyethylene glycol dimethyl ether)	0.02**		
Formate	49		
Iron, as $Fe(CO)_5$	5	0.01	0.1
Nickel, as $Ni(CO)_4$	1	0.01	0.1

*Much higher levels have been reported. Limit set based on apparent economic operating range of guard bed materials.

**Based on a vapor pressure of 0.0007 mm Hg at 77°F, and assuming no entrainment of liquid.

SUMMARY AND CONCLUSIONS:

1. Seven adsorbents including active carbons, silica gel, alumina, H-Y zeolite, and spent methanol catalyst were screened for $Fe(CO)_5$ adsorption. The $Fe(CO)_5$ adsorption capacity of the adsorbents decreased in the order: active carbon > H-Y zeolite > silica gel > alumina > spent methanol catalyst.

2. The effect of temperature on $Fe(CO)_5$ adsorption was investigated on adsorbents H-Y zeolite and BPL carbon. It was determined that the effect of temperature on $Fe(CO)_5$ adsorption is quite marked. The apparent heat of $Fe(CO)_5$ adsorption from 40 psig carrier (73% CO_2/70% N_2/1% CO) on H-Y at low surface coverage is about 13 kcal/mole, while that value for BPL is about 20 kcal/mole. These high heats of adsorption indicate that $Fe(CO)_5$ capacity can be significantly enhanced by reducing the adsorption temperature. In addition, the apparent heat of $Fe(CO)_5$ adsorption on both H-Y and BPL carbon decreased as surface coverage increased, indicative of adsorbent heterogeneity.

3. The effect of carrier gas composition on $Fe(CO)_5$ adsorption was also investigated. It was determined that the presence of CO_2 in the carrier gas stream produced reductions in $Fe(CO)_5$ capacity. At 100°F and 40 psig total pressure, the equilibrium capacities of BPL and H-Y at 5 ppm $Fe(CO)_5$ were reduced 30% and 50% respectively as the carrier gas composition was changed from 95% N_2/5% CO to 73% CO_2/26% N_2/1% CO.

4. The effect of thermal regeneration on $Fe(CO)_5$ adsorption was studied because the $Fe(CO)_5$ adsorption capacities of BPL and H-Y are too low for throw-away application. Thermal regeneration of BPL in N_2 at 250°F after $Fe(CO)_5$ adsorption showed that 25% of the adsorption capacity was lost after regeneration. On the other hand, H-Y zeolite showed the same percentage of $Fe(CO)_5$ after three adsorption/regeneration cycles.

5. The effect of carrier gas pressure on $Fe(CO)_5$ adsorption was also studied. As the carrier gas pressure increased from 40 to 90 psig, the $Fe(CO)_5$ capacities of both BPL and H-Y were reduced. For BPL, as the carrier gas pressure increased from 40 to 90 psig, the $Fe(CO)_5$ capacity at 75°F and 5 ppm was reduced by 55%. The corresponding reduction in H-Y capacity was 65%.

6. A mixed Langmuir approach was used to estimate the $Fe(CO)_5$ capacity on H-Y. This approach underpredicted the $Fe(CO)_5$ capacity on H-Y by approximately 40%, indicating that using the mixed Langmuir theory to estimate adsorption capacities at higher carrier gas pressure will give conservative estimates of capacity.

7. Adsorption of trace $Ni(CO)_4$ was measured on BPL and H-Y. The capacity for $Ni(CO)_4$ on both adsorbents is significantly less than that for $Fe(CO)_5$. From 40 psig carrier (95% N_2/5% CO) at 75°F and 1 ppm equilibrium concentration, the $Ni(CO)_4$ capacities are 2.7 and 3.4 times lower than those for $Fe(CO)_5$ for BPL and H-Y, respectively.

8. The effect of temperature on $Ni(CO)_4$ adsorption on BPL and H-Y was investigated. As in the case of $Fe(CO)_5$ adsorption, the apparent $Ni(CO)_4$ heat of adsorption is quite large, about 17 and 12 kcal/mole at low surface coverage for BPL and H-Y, respectively. This indicates that $Ni(CO)_4$ capacity can be enhanced significantly by reduction in adsorption temperature. Also, each adsorbent demonstrates energetic heterogeneity with respect to $Ni(CO)_4$ adsorption as noted by the decrease in apparent heat of adsorption with increasing surface coverage.

9. The effect of carrier gas pressure on $Ni(CO)_4$ adsorption was investigated. Increasing the carrier gas pressure from 40 to 90 psig at 75°F caused a decrease in $Ni(CO)_4$ capacity. The $Ni(CO)_4$ capacity of BPL at 1 ppm decreased by a factor of 4 as the carrier gas pressure increased from 40 to 90 psig. This decrease is larger than that noted with $Fe(CO)_5$ adsorption which is expected since $Fe(CO)_5$ is more strongly adsorbed than $Ni(CO)_4$.

10. Thermal regeneration studies on $Ni(CO)_4$ adsorption on BPL carbon showed that regeneration in N_2 at 250°F was sufficient to completely restore the $Ni(CO)_4$ capacity.

11. The adsorption of trace COS was measured on eight different adsorbents at 75°F from 90 psig carrier. These adsorbents included BPL, H-Y, various metal oxide loaded carbons, a metal oxide promoted alumina, a metal oxide promoted zinc oxide, and spent methanol catalyst. The adsorption capacities for those adsorbents decrease in the order: FCA carbon (copper oxide/chromium oxide loaded carbon) > spent methanol

catalyst > BPL > H-Y. Both adsorbents with high COS capacity contain copper.

12. It was determined that FCA carbon could be regenerated in N_2 at 500°F to restore its COS capacity.

13. The apparent heat of COS adsorption is ~13 kcal/mole at low surface coverage, indicating that adsorption temperature will have a large effect on COS capacity. The reduction in heat of adsorption with increasing surface coverage denotes adsorbent heterogeneity.

14. Nine adsorbents were screened for trace H_2S adsorption at 75°F and 90 psig. The adsorbents screened include two zeolites, active carbon, three impregnated carbons, two spent methanol catalysts, and a promoted zinc oxide. All adsorbents that contain copper demonstrate high H_2S capacity. The capacity of these materials decrease in the order: BASF S3-85 > EPJ-19 > FCA > desulf 12. The impregnated carbons, FCA and desulf 12, are steam regenerable, while the spent methanol catalysts, BASF S3-85 and EPJ-19, would be throw-away adsorbents.

15. Removal of COS and H_2S with zinc oxide at elevated temperature was investigated. Using HTZ-4 at 400°F and 90 psig, the H_2S capacity was determined to be ~3.0 mmole/g. In addition, hydrolysis of COS occurred readily at these conditions. The appeal of this system for H_2S and COS removal is that it is a throw-away system, and the COS capacity is significantly higher than that noted for ambient temperature systems.

16. Seven adsorbents were screened for trace HCl adsorption at 75°F and 90 psig. The adsorbents screened include H-Y, BPL, metal oxide loaded carbons, spent methanol catalysts, and a metal oxide promoted alumina. The capacity of the spent methanol catalyst, S3-85, is highest followed by FCA carbon. The adsorption capacity of S3-85 at 5 ppm is 7.4 mmole/g which is sufficient for a throw-away adsorbent.

17. The results of adsorbent screening have led to a conceptual low temperature adsorption poison removal design. The first adsorbent bed would contain spent methanol catalyst to adsorb H_2S and HCl in a throw-away system. The next bed would contain H-Y for $Fe(CO)_5$ removal, followed by BPL for $Ni(CO)_4$ removal, and finally FCA carbon for COS removal. The H-Y, BPL, and FCA sections are thermally regenerable at 500°F. This design will be tested at the pilot unit scale with actual coal gasifier off-gas.

PATENT SITUATION:

To our best knowledge, there are no patentable concepts forthcoming from this work. All adsorbent materials investigated are commercially available and the process cycle is either conventional temperature swing adsorption (TSA) or throw-away. Nonetheless, the poison removal designs may contain patentable ideas, particularly with respect to the preferred sequence of adsorbents for efficient poisons removal.

SAFETY:

The primary hazard associated with this project is the toxic nature of the catalyst poisons. $Fe(CO)_5$, $Ni(CO)_4$, H_2S, COS, and HCl have TLV's of 0.1, 0.05, 10, 10, and 5 ppm, respectively. In addition, $Ni(CO)_4$ is a suspected carcinogen. In order to avoid exposure to these compounds, a number of precautions were taken: 1) placing the recirculating adsorption apparatus in a walk-in hood, 2) equipping the system with a low pressure pump shut-off in case of a system leak, 3) the poison concentration and total gas volume were kept low, 4) all vent lines in the system containing the poisons were scrubbed before venting in the hood, and 5) in all $Ni(CO)_4$ experiments, an air-line respirator was employed.

FUTURE PROGRAMS:

The results of this work will be used to design a poisons removal pilot unit, which will test the design concept for removal of catalyst poisons from coal gasifier off-gas. The pilot unit test will investigate interactions, if any, between catalyst poisons and adsorbent deactivation rates.

ACKNOWLEDGMENTS:

The author would like to thank K. E. Snyder for her excellent technical support in all phases of this work. In addition, the support and ideas of T. H. Hsiung and the support of D. Grieble, J. Phillips, K. Tewari, P. Maroulis, and J. Wallace in CRSD Analytical are gratefully noted.

EXPERIMENTAL APPARATUS AND PROCEDURES:

Equilibrium and kinetic adsorption measurements were measured volumetrically in a recirculating adsorption apparatus (Figure 1). The unit had previously been used to screen adsorbents for landfill gas pretreatment, and was modified considerably for these experiments (2). The recirculating adsorption apparatus was used because it offers a number of advantages over measuring adsorption capacities and kinetics by breakthrough experiments. Since the MTZ for removal of trace impurities is long, breakthrough experiments require a large volume of gas and a long time for complete breakthrough to occur. In addition, equilibrium capacity for only one concentration can be obtained at the conclusion of the experiment. The recirculating apparatus, on the other hand, requires a minimal amount of gas which is highly desirable due to the toxicity and carcinogenicity of the impurities studied. A complete isotherm can be measured in the span of a few days and by monitoring the approach to equilibrium as a function of time, mass transfer coefficients can be obtained. From these mass transfer coefficients, MTZs can be calculated. Hence, the recirculating adsorption apparatus is very economical with respect to time required for data generation and gas consumption.

The recirculating adsorption apparatus is primarily constructed of stainless steel 1/4 inch tubing and a Teflon diaphragm pump. The Teflon pump was chosen because it exhibits little adsorption affinity for the impurities studied. Due to the toxicity of the impurities studied, the recirculating apparatus and all gas supplies were located in a walk-in hood. The unit is supplied with house nitrogen. Poison gas blends are equipped with a nitrogen purge captured vent flammable gas regulator. An ASCO solenoid valve (normally closed) is

FIGURE 1

Recirculating Adsorption Test Apparatus

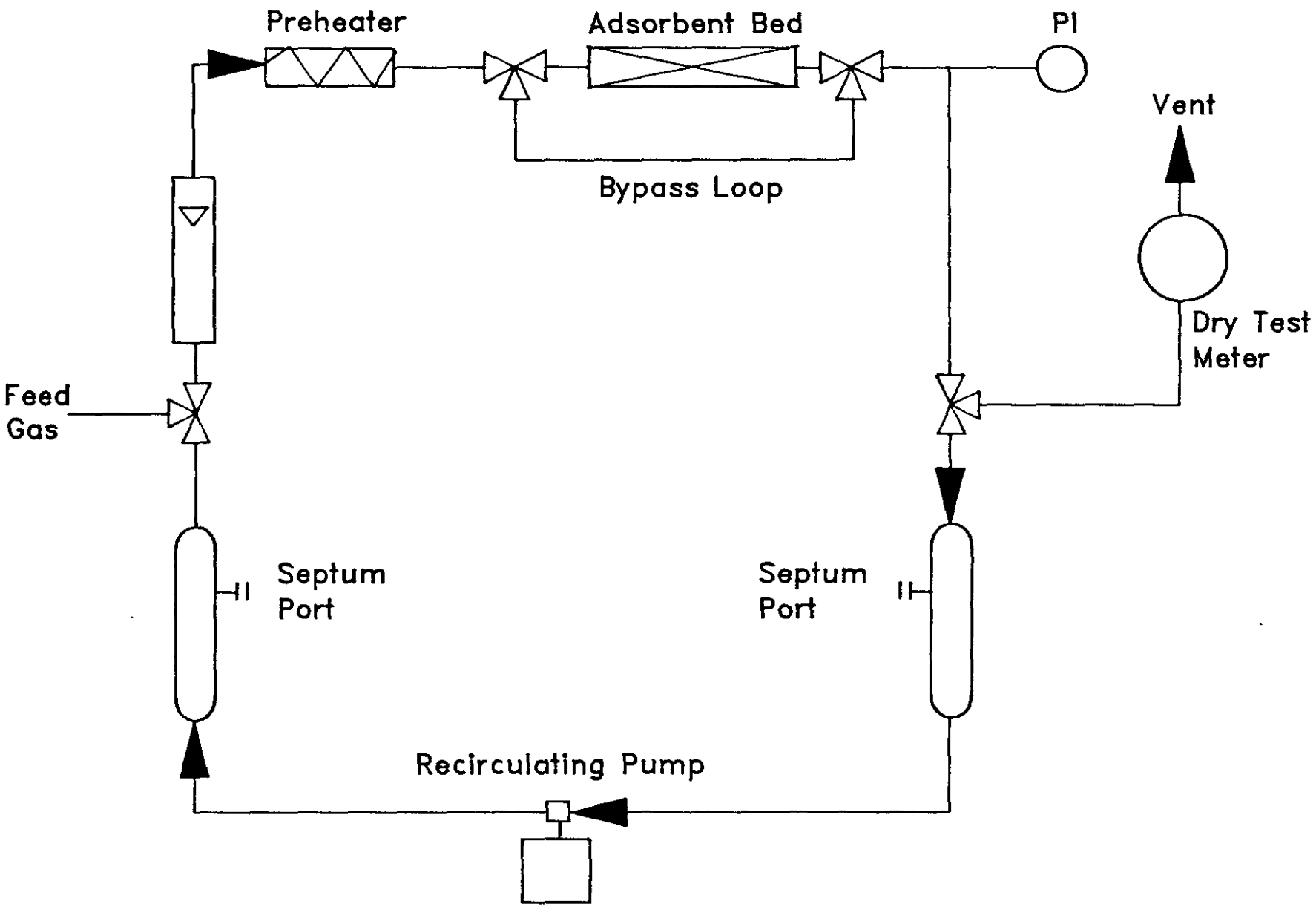

located on the feed line. It is configured to close in the event of a hood or electrical failure. Poison gases are introduced to the recirculating loop via Feed #2 regulator. The feed line is equipped with an excess flow valve which will close in the event of a pressure surge or excessive flow. Carbon dioxide, nitrogen, and other diluent gases are introduced via Feed #1 and #3 connections.

All gases vented from the system are scrubbed through a bubbler system or a heated packed bed to decompose the poisons in the gas stream. In the case of iron and nickel carbonyls, this consists of passing the gas stream through a 6 to 10 inch bed of alumina heated to 300°C. This decomposes the metal carbonyls liberating carbon monoxide and depositing iron or nickel metal on the alumina. Carbonyl sulfide and hydrogen sulfide are scrubbed through a bubbler system filled with two molar sodium hydroxide and phenolpthalein indicator. This converts the material to sodium sulfide and water. Similarly, hydrogen chloride is scrubbed through a two molar solution of sodium hydroxide, producing sodium chloride and water on decomposition.

The recirculating adsorption apparatus is equipped with three heated zones: a preheater, adsorption bed heater, and a bar heater. Each is controlled by an ECS controller and alarm card. There is a high/low pressure alarm in the recirculating loop configured to shut down the pump, solenoid, and heated zones should pressures drop below 25 psi or exceed 105 psi. A hood failure alarm of the differential pressure sensing type continuously monitors air flow through the hood. In the event of a failure, an audible alarm sounds and the power to the solenoid on the pump nitrogen supply line and ASCO solenoid on the poison feed line is interrupted.

A typical experiment in the recirculating apparatus was run as follows:

1. A sample of adsorbent was regenerated with nitrogen at 150 to 400°C (dependent upon the adsorbent) to a dew point of less than -40°C while in the adsorption bed.

2. Using the inlet feed system, the adsorption loop was pressurized to 90 psig with carbon dioxide and isolated.

3. The recirculating loop was then vented to atmospheric pressure. The loop was closed, filled with 1 atmosphere of trace impurity, and finally filled to 90 psig with carbon dioxide. In the actual pretreatment bed, the impurities will be adsorbed from a synthesis gas matrix (CO, H_2, N_2, CO_2). For experimental simplification, all runs were done with CO_2 only. Since CO_2 is the most strongly adsorbed of all the components in the matrix, the data obtained from CO_2 should provide a good estimate of capacities in the actual synthesis gas matrix. The pressure of 90 psig was chosen because it reflects the partial pressure of CO_2 at process operating conditions.

4. After recirculating for about 10 minutes to ensure good mixing, the concentration in the recirculating loop was determined by withdrawing a 1 cc sample at the sampling port and injecting into the gas chromatograph. The GC employed in this study was a Hewlett Packard 5890A. The volume of the sample withdrawn (1 cc) was much less than the total system volume (4 liters). In the case of HCl, continuous on-line

analysis was done using a Nicolet 1000 meter cell FTIR installed directly in the recirculating loop. The system volume was 9 liters.

5. Once the concentration in the recirculating loop was known, the gas was directed to the adsorption bed with valves V-16 and V-17.

6. The impurity concentration in the gas stream was then monitored as a function of time yielding data on the kinetics of adsorption.

7. After equilibrium was reached and the final impurity concentration was known, the adsorption bed was isolated using valves V-16 and V-17.

8. Another adsorption point or desorption point was obtained by increasing or decreasing the impurity concentration in the recirculating loop and following step 3-7. The adsorbate concentration in the recirculating loop was decreased by purging with CO_2.

Analytical Techniques

A packed column gas chromatograph equipped with an electron capture detector (ECD) was used to analyze both nickel and iron carbonyl. For determination of COS and H_2S, a packed column gas chromatograph equipped with a photoionization detector (PID) was employed. Specifics about the analytical techniques including column packings, carrier gas flowrates, temperatures as well as sample chromatograms for carbonyl and sulfur determination are given in Appendix A.

RESULTS AND DISCUSSION:

Adsorption of $Fe(CO)_5$

Equilibrium Capacity of Various Adsorbents at 100°F

A number of commercially available adsorbents were screened for their $Fe(CO)_5$ adsorption capacity at 100°F and 40 psig (5% CO, 95% N_2). These adsorbents included three activated carbons, silica gel, activated alumina, H-Y zeolite, and spent methanol catalyst. Some of the pertinent physical properties of these adsorbents are given in Table 2.

The $Fe(CO)_5$ adsorption isotherms on the seven adsorbents screened initially are given in Figure 2. As clearly noted from the isotherms, the activated carbons and the zeolite show significantly higher adsorption capacities than silica gel, alumina, or spent methanol catalyst. Consequently, the activated carbons and H-Y zeolites were further screened for $Fe(CO)_5$ removal. Several variables including the effect of temperature, total carrier gas pressure, and thermal regenerability of the adsorbents were investigated.

It is interesting to note that the $Fe(CO)_5$ capacity and Henry's law constants (initial isotherm slopes) for the adsorbents increase as the surface area of the adsorbent increases. As the microporosity of an adsorbent increases so does its surface area, thus the adsorption capacity for $Fe(CO)_5$ is also enhanced. This is true for adsorbents with very different surface polarities like carbons and zeolites. This suggests that adsorption of

TABLE 2

Physical Properties of Adsorbents for $Fe(CO)_5$ Adsorption

Adsorbent	Manufacturer	(m^2/g) Surface Area	(lbs/ft^3) Bulk Density	(A) Average Pore Diameters
BPL Carbon	Calgon	1100	30.0	20
PCB Carbon	Calgon	1200	27.4	15
CAL Carbon	Calgon	1000	25.0	25
Silica Gel, Grade 40	Davison	750	46.0	22
Activated Alumina, S-100	Alcoa	340	45.0	60
Methanol Catalyst, EPJ-19	United Catalysts	100	80.0	-
H-Y Zeolite	Linde	900	42.0	10

FIGURE 2

Fe(CO)5 adsorption at 100 F, 40 psig

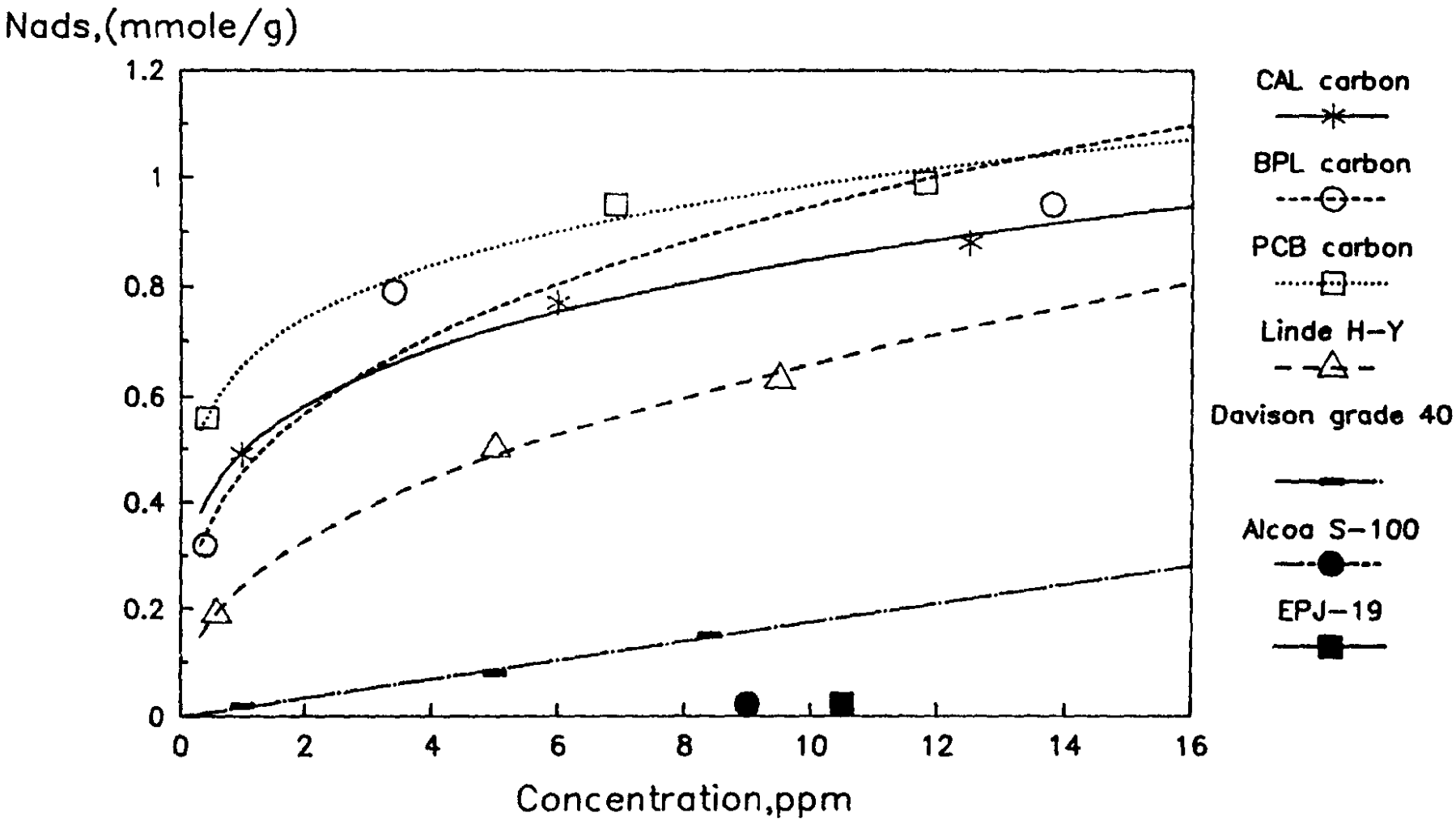

$Fe(CO)_5$ on these adsorbents is dominated by the nature of the pore structure and less effected by the chemical nature of the surface.

Effect of Carrier Gas on $Fe(CO)_5$ Adsorption

The composition of carrier gas has a large effect on the adsorption of trace compounds. As the strength of adsorption between adsorbent and carrier gas increases, the extent of adsorption of the trace impurity decreases. Consequently, the effect of CO_2 carrier gas on the adsorption of $Fe(CO)_5$ on activated carbon and H-Y zeolite was investigated. Of all the compounds present in synthesis gas, CO_2 is most strongly physically adsorbed and therefore its effect was investigated.

Figures 3 and 4 show the effect of CO_2 on the adsorption of $Fe(CO)_5$ on BPL carbon and H-Y zeolite. The reason H-Y zeolite was chosen for this application is that its affinity for CO_2 is much less than that for other zeolites like 13X. It is clear from the isotherms that the presence of CO_2 does reduce the $Fe(CO)_5$ capacity of both adsorbents. The capacities of BPL carbon and H-Y zeolite are reduced by about 30% and 50%, respectively, at an equilibrium concentration of 5 ppm $Fe(CO)_5$. The reduction in capacity is greater for the zeolite because CO_2, which is a polar molecule, is adsorbed more strongly on the polar zeolite than the non-polar carbon.

Effect of Temperature on $Fe(CO)_5$ Adsorption at 40 psig

The effect of temperature on $Fe(CO)_5$ adsorption on H-Y zeolite and BPL carbon was investigated. Since adsorption is an exothermic process, the

FIGURE 3

Effect of CO2 on Fe(CO)5 Adsorption on BPL

100 F, 40 psig

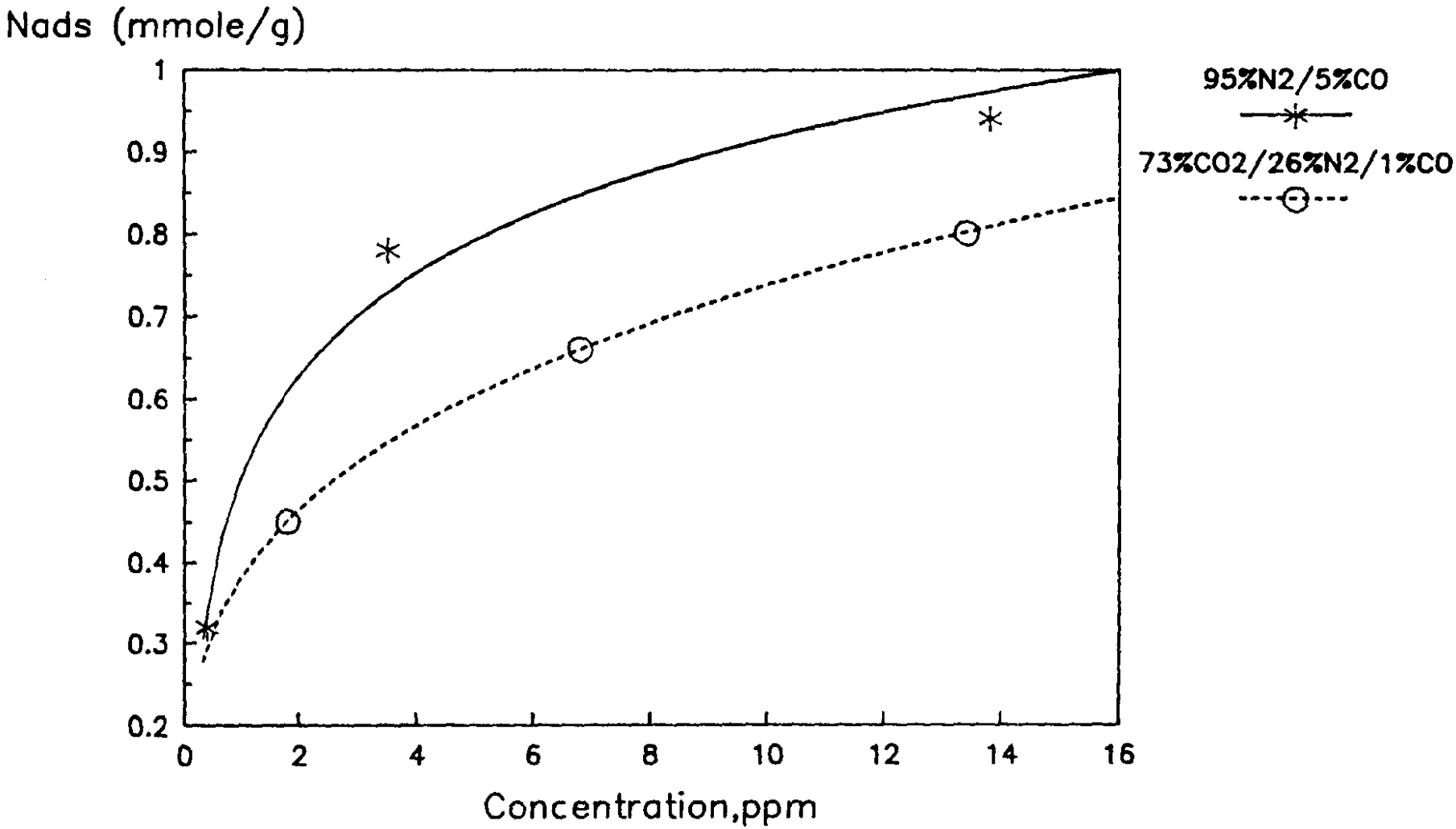

FIGURE 4

Effect of CO2 on Fe(CO)5 Adsorption on H-Y

100 F, 40 psig

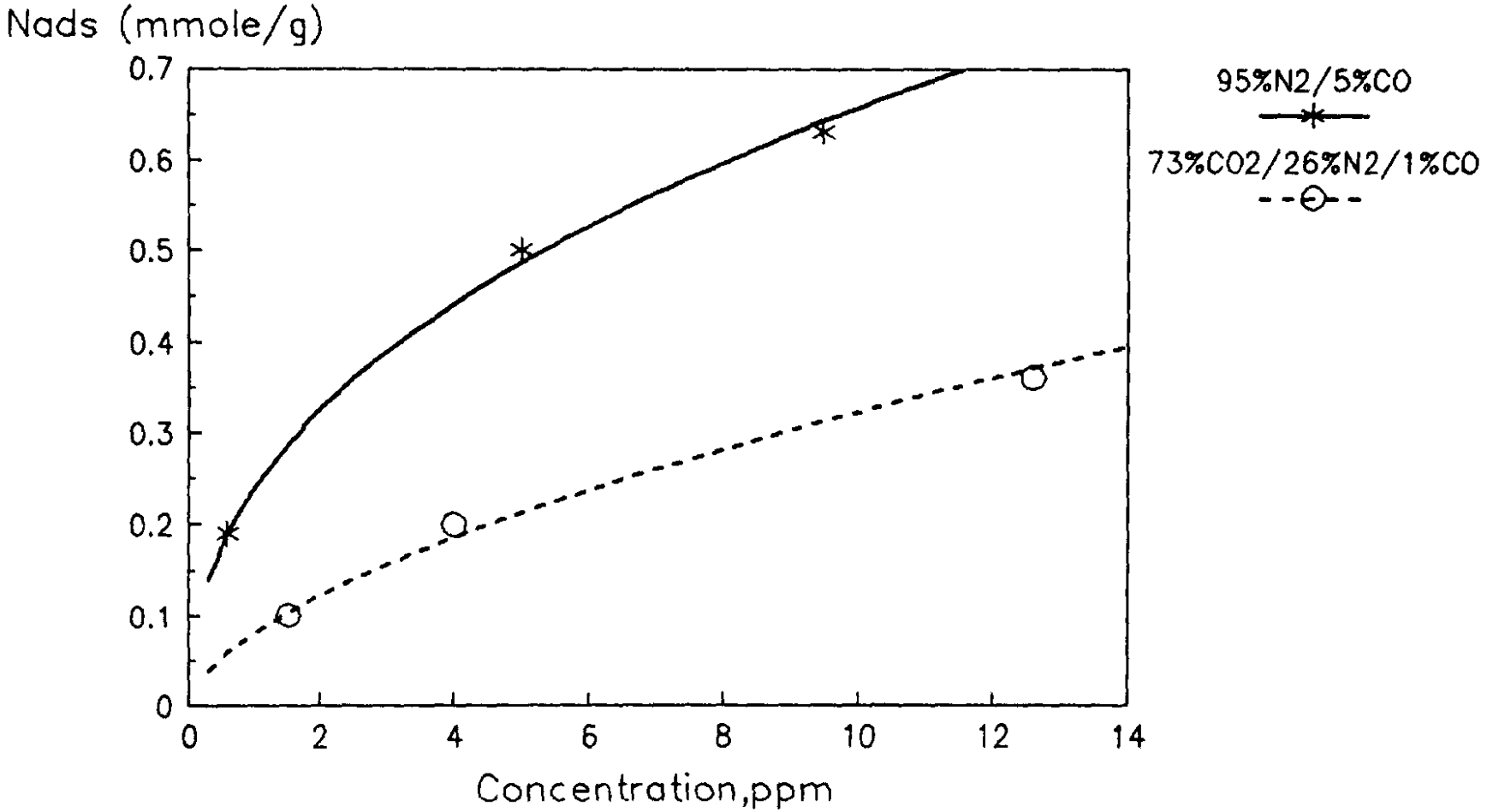

extent of adsorption increases as the temperature decreases. Using the Clausius-Clayperon equation, the isosteric heat of adsorption of a given species can be calculated from isotherms at two different temperatures. The working equation is:

$$\ln(P_1/P_2)\eta = qst/R\ (1/T_1 - 1/T_2)$$

where P_1 and P_2 are the partial pressures of the adsorbate at a given amount adsorbed at absolute temperatures T_1 and T_2. qst is the isosteric heat of adsorption and R is the gas constant. In addition, once the heat of adsorption is known as a function of the amount adsorbed, adsorption isotherms at other temperatures can be calculated. It should be emphasized that use of the Clausius-Clayperon equation is strictly thermodynamically correct for pure components only. Hence, the heat of adsorption calculated from mixture data is an "apparent" heat of adsorption. Nonetheless, the technique is useful in estimating the effect of temperature on adsorption.

Figures 5 and 6 show $Fe(CO)_5$ adsorption isotherms at 100 and 75°F from 40 psig (73% CO_2/26% N_2/1% CO) carrier on H-Y and BPL, respectively. In each figure the apparent heat of adsorption as a function of surface coverage is given.

Figure 5 shows that the apparent heat of $Fe(CO)_5$ adsorption on Linde H-Y under the given conditions is 12.5 kcal/mole at a surface coverage of 0.10 mmole/g and reduces to 9.6 kcal/mole at 0.30 mmole/g. First, the magnitude of the apparent heat of adsorption is rather large. This indicates that the adsorption of $Fe(CO)_5$ is very sensitive to temperature. For

FIGURE 5

Fe(CO)5 Adsorption at 100 and 75 F on H-Y

40 psig (73%CO2/26%N2/1%CO)

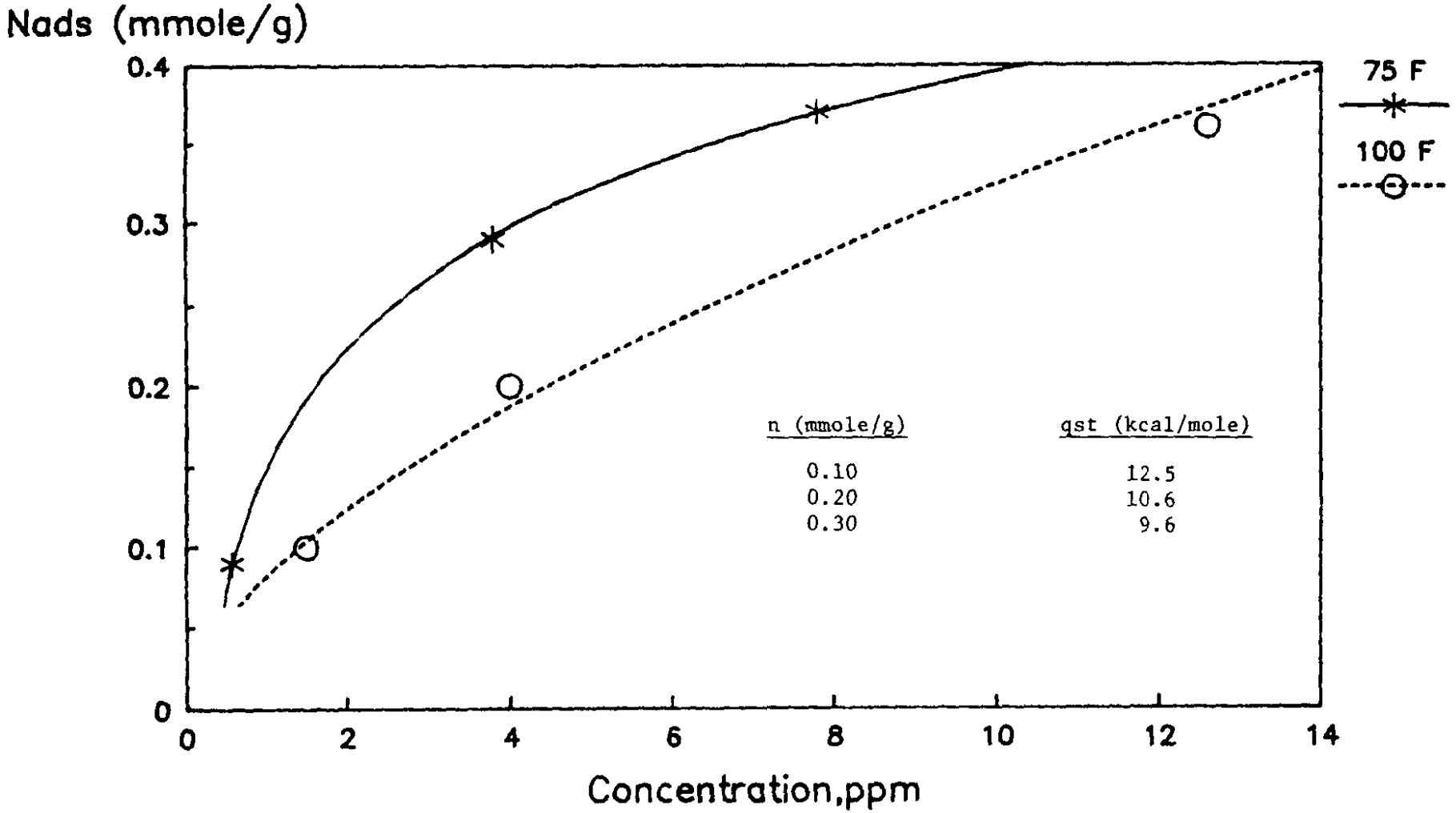

FIGURE 6

Fe(CO)5 Adsorption at 100 and 75 F on BPL

40 psig (73%CO2/26%N2/1%CO)

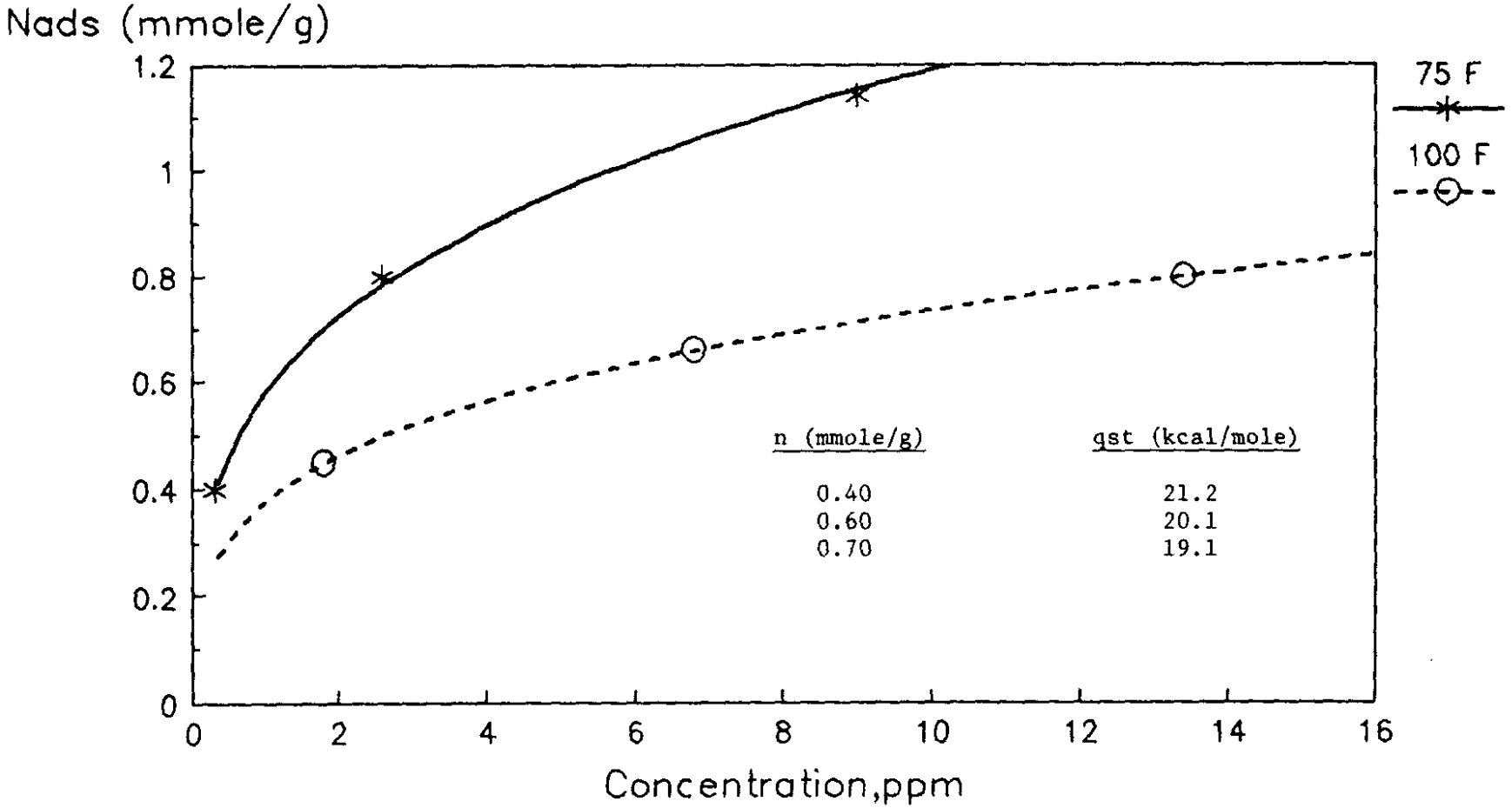

example, at 100°F the adsorption capacity at an equilibrium concentration of 5 ppm is 0.22 mmole/g, while at 75°F that value increases almost 50% to 0.32 mmole/g. Thus, the extent of $Fe(CO)_5$ adsorption can be significantly modified by changing the adsorption temperature. Second, the decrease in apparent heat of adsorption with increasing surface coverage indicates adsorbent heterogenity with respect to $Fe(CO)_5$ adsorption.

Figure 6 shows $Fe(CO)_5$ adsorption isotherms at 100 and 75°F on BPL carbon. Adsorption of $Fe(CO)_5$ on BPL carbon shows greater temperature sensitivity than that on H-Y zeolite as noted by its higher apparent heat of adsorption. The magnitude of the heat of adsorption, ~20 kcal/mole, is very high suggesting that $Fe(CO)_5$ may be chemisorbed on the carbon surface. The heat of adsorption of a compound is an indication of the strength of the adsorption bond. Clearly, $Fe(CO)_5$ is adsorbed more strongly on BPL carbon than H-Y zeolite as evidenced by its adsorption capacity, Henry's law constant and heat of adsorption. The Henry's law constant of an isotherm is proportional to the heat of adsorption. At an equilibrium concentration of 5 ppm, the $Fe(CO)_5$ adsorption capacity at 100°F is 0.62 mmole/g, while at 75°F that value is 0.96 mmole/g. Hence, due to the high heat of adsorption of $Fe(CO)_5$ on both H-Y and BPL, the adsorption capacity can be significantly enhanced by reducing the adsorption temperature.

Thermal Regeneration Studies

The adsorption capacity of BPL carbon at 75°F and 40 psig carrier (73% CO_2/26% N_2/1% CO) is 0.96 mmole/g at an equilibrium concentration of 5 ppm. For a methanol plant with an inlet flow rate of 40 MMSCFD (100 TPD

methanol), the calculated weight of BPL carbon needed to remove 5 ppm $Fe(CO)_5$ based on the above capacity is about 500 lbs of carbon per day. This carbon utilization rate is too expensive for a throw-away adsorbent. Subsequently, regeneration experiments were carried out to determine 1) if the adsorptive capacity of the adsorbents are recovered after thermal regeneration, 2) what temperature is required to regenerate the adsorbent, and 3) if all the carbonyl impurity is desorbed as such or if metal species are deposited on the adsorbent surface.

Figure 7 shows $Fe(CO)_5$ adsorption isotherms on BPL carbon at 75°F from 40 psig carrier (73% CO_2/26% N_2/1% CO) on successive runs following regeneration in N_2 at 250°F. It can be noted that the $Fe(CO)_5$ capacity of BPL is reduced on each successive run following regeneration in N_2 at 250°F. The $Fe(CO)_5$ adsorption capacity at 5 ppm decreases from 0.96 to 0.77 mmole/g following two regeneration cycles.

To help elucidate the cause of this adsorbent deactivation, the gas effluent during regeneration in N_2 was monitored for $Fe(CO)_5$ concentration. By knowing the gas effluent rate and the $Fe(CO)_5$ effluent concentration as a function of time, a desorption curve can be obtained. From this desorption curve, the total quantity of $Fe(CO)_5$ desorbed from the adsorbent can be determined. The $Fe(CO)_5$ desorption curve for BPL carbon is shown in Figure 8. Since the $Fe(CO)_5$ loading of the adsorbent prior to regeneration was known and the total quantity of $Fe(CO)_5$ desorbed can be calculated from the desorption curve, the amount of iron remaining on the carbon surface can be calculated by subtraction.

FIGURE 7

Effect of Regeneration on Fe(CO)5 Capacity

75 F and 40 psig on BPL

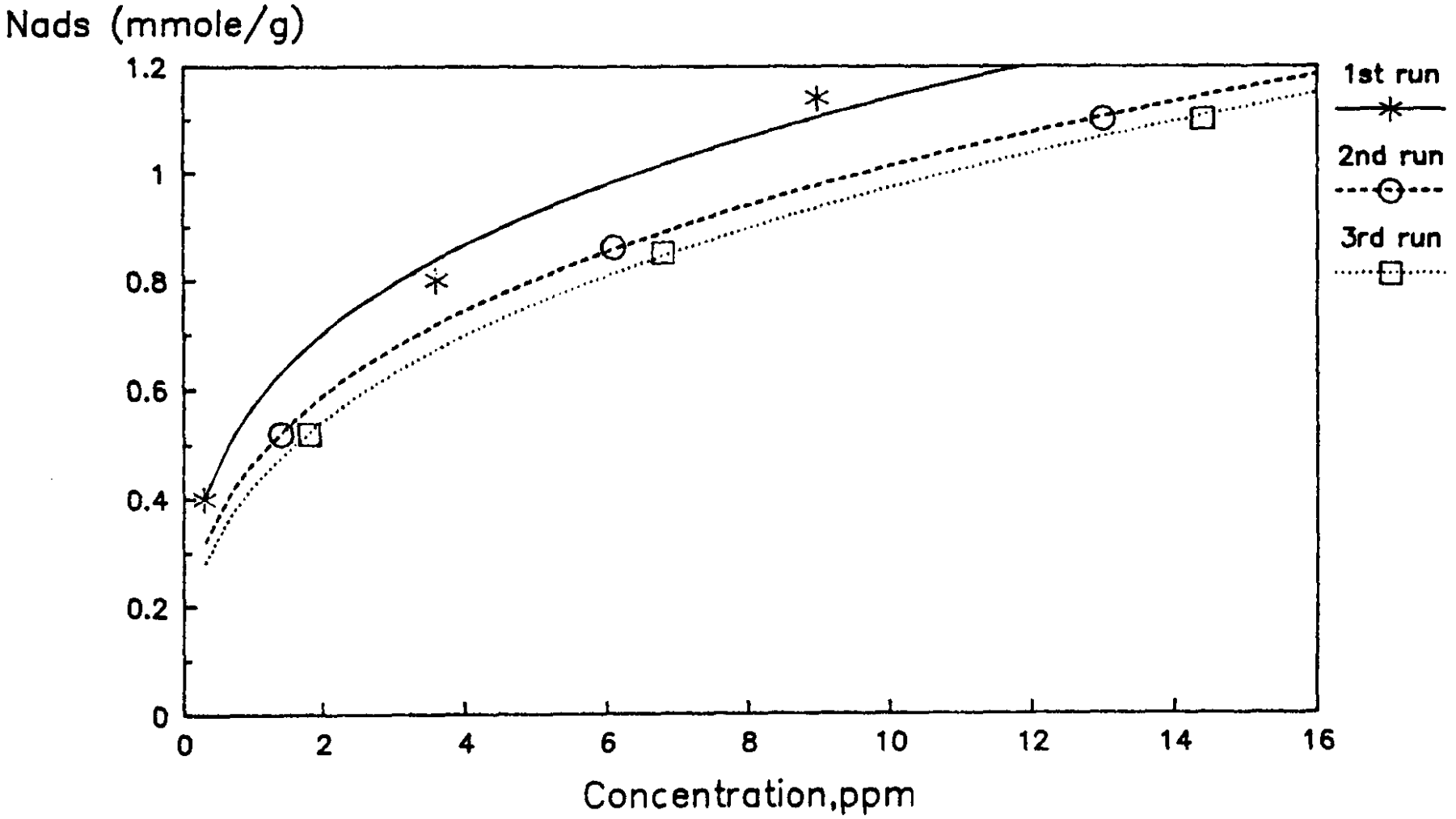

FIGURE 8

Fe(CO)5 Thermal Desorption Curve on BPL

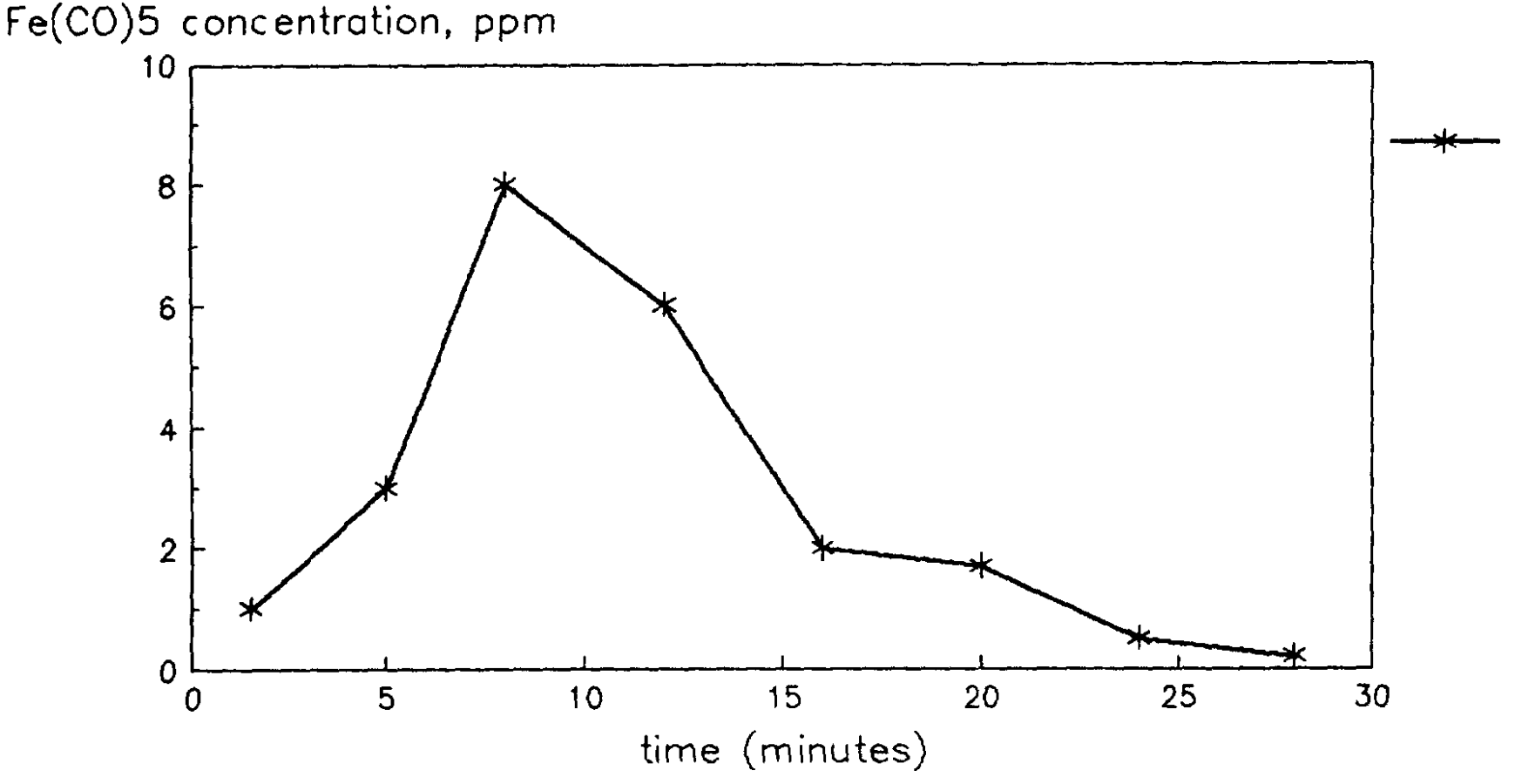

heat rate = 10 F/min
flow rate = 1 liter/min
250 F final temperature

A number of points can be made concerning thermal adsorption of $Fe(CO)_5$ from active carbon. Very little adsorbed $Fe(CO)_5$ is desorbed as $Fe(CO)_5$. The desorption curves indicate that less than 0.1 (wt%) of $Fe(CO)_5$ is desorbed as such. This means a large fraction of some iron species remains on the carbon surface. It is strongly suspected that the iron species is iron metal even though 250°F is below the decomposition temperature (300°F) of $Fe(CO)_5$. Adsorbed $Fe(CO)_5$ can decompose before the decomposition temperature of the pure compound because they are two different thermodynamic species. The "spent" adsorbent is weighed after regeneration and the weight increase is noted. In order to close the mass balance, the weight increase must be done to elemental iron. In addition, other studies on the adsorption of $Fe(CO)_5$ on adsorbents indicate that elemental iron is left on the adsorbent surface following thermal regeneration in this temperature range (3). Other interesting experimental observations which suggest elemental iron is formed in the ferromagnetic nature of the spent adsorbent which is readily attracted to a bar magnet. In addition, both CO and CO_2 are evolved during the thermal decomposition step. It is well known that elemental iron is a catalyst for the Bouduoard reaction at low temperatures (100°C) ($2\ CO \longrightarrow CO_2 + C$)(4). Thus, CO evolved during decomposition of $Fe(CO)_5$ must react in the presence of elemental iron and form CO_2 and deposit carbon. Thus, thermal regeneration studies on active carbon following $Fe(CO)_5$ adsorption demonstrate 1) $Fe(CO)_5$ adsorption capacity is reduced following thermal regeneration, and 2) thermal regeneration leads to deposition of elemental iron on the surface of the carbon which is most likely the reason for the loss of adsorption capacity.

Figure 9 shows $Fe(CO)_5$ adsorption isotherms on Linde H-Y zeolite at 75°F from 90 psig carrier (73% CO_2/26% N_2/1% CO) on successive runs following regeneration in N_2 at 250°F. It is noted that for three successive adsorption/regeneration cycles, the zeolite demonstrates the same adsorptive capacity. A desorption curve similar to that for BPL was measured as shown in Figure 10. It can be noted that significantly more $Fe(CO)_5$ is desorbed from the zeolite than the carbon. However, the total quantity of $Fe(CO)_5$ desorbed is equal to about 30% of that adsorbed. Once again the iron species on the "spent" adsorbent seems to be elemental iron as indicated by mass balance requirements, the ferromagnetic property of the spent adsorbent, and previous investigations of $Fe(CO)_5$ adsorption and decomposition on H-Y zeolite (3).

This raises the question as to why the equilibrium capacity remains the same while iron species are deposited on the zeolite surface? A possible explanation is that the adsorbed $Fe(CO)_5$ in the zeolite pores migrates into the macroporous binder of the zeolite during thermal regeneration. The macropores of the zeolite don't contain significant adsorption capacity. However, diffusion in pelletized zeolites is limited by macropore diffusion. The primary reason for this is the much smaller size of the microporous zeolite crystals (1-10 microns) versus the size of the macroporous binder network (1-2 mm). Hence, if deposition occurs in the macropores, the rate of $Fe(CO)_5$ adsorption should decrease. Figure 11 shows the fractional approach to equilibrium as a function of time on three successive adsorption/regeneration cycles. As depicted in the figure, the approach to equilibrium is slowed with each successive adsorption/regeneration cycle. In addition, previous researchers have shown that the iron crystallites present

FIGURE 9

Effect of Regeneration on Fe(CO)5 Capacity

75 F and 40psig on H-Y

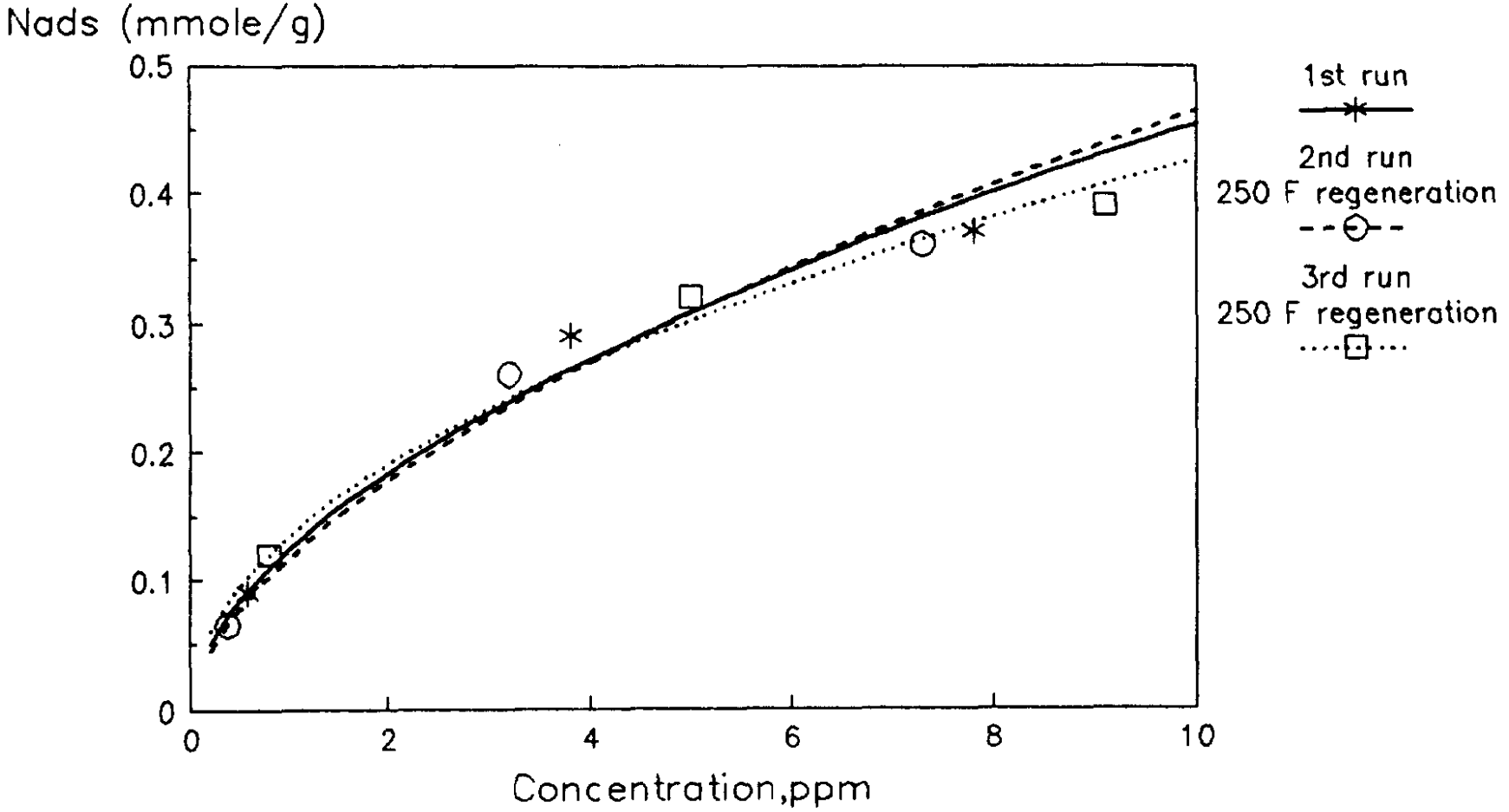

FIGURE 10

Fe(CO)5 Thermal Desorption Curve on H-Y

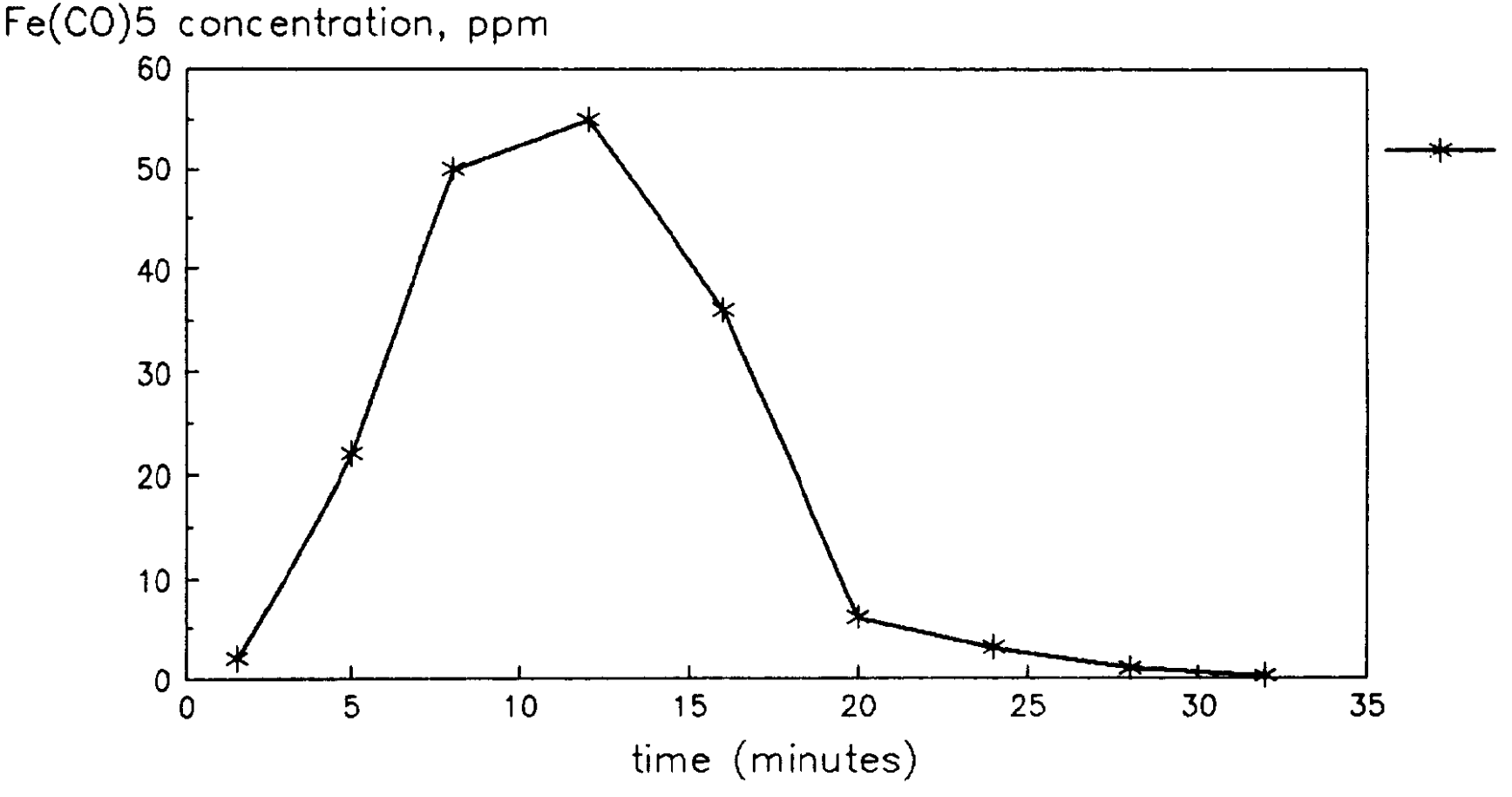

heat rate = 10 F/min
flow rate = 1 liter/min
250 F final temperature

FIGURE 11

Fe(CO)5 Uptake Curves on H-Y

75 F and 40 psig

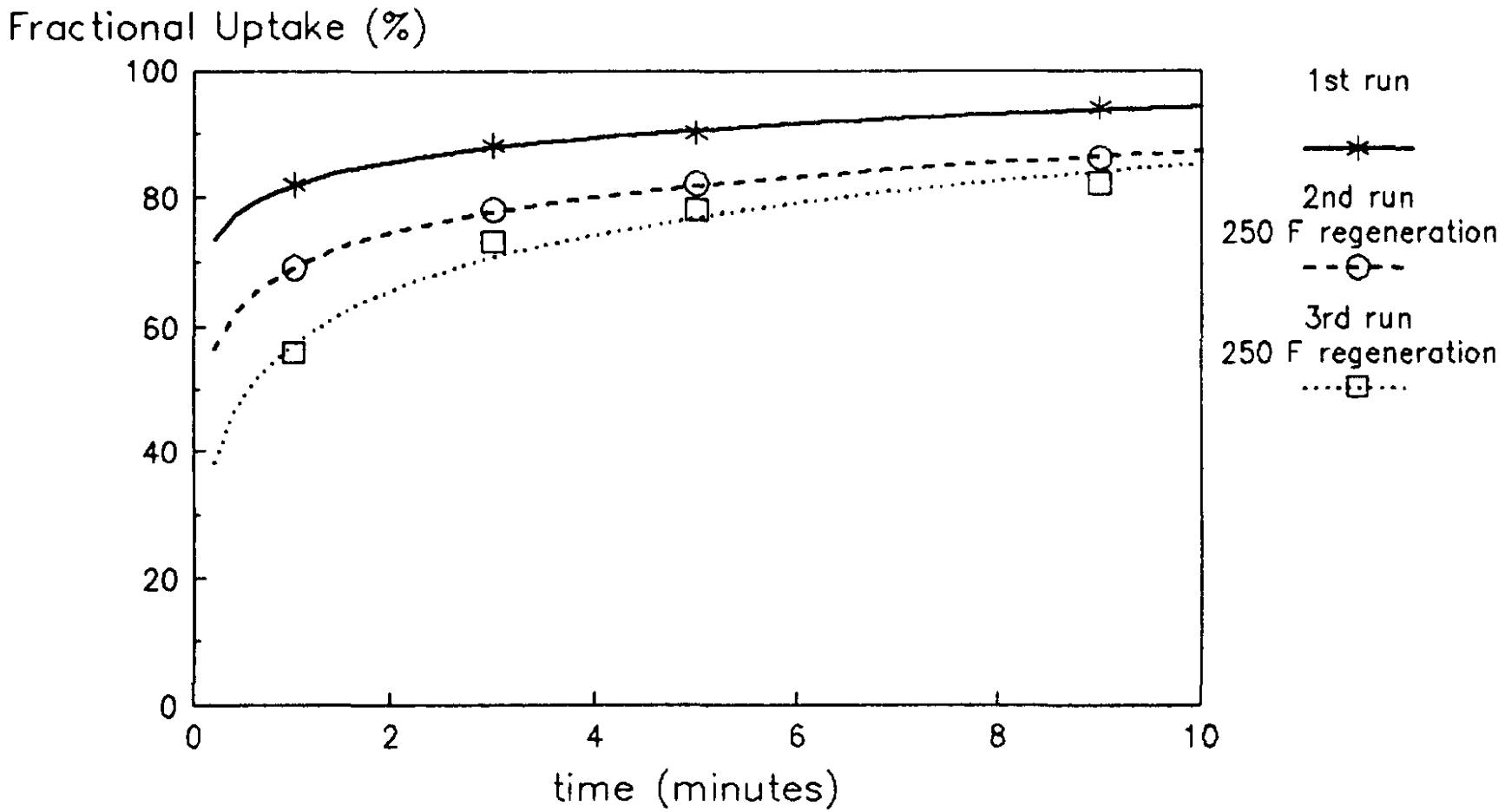

in H-Y zeolite following thermal regeneration of $Fe(CO)_5$ are larger than 12A (3). The pore size of H-Y zeolite is ~10A, therefore, it is not expected that much larger iron species are present within the zeolite structure. This suggests that the deposited iron species is outside the zeolite structure.

The thermal desorption curve of H-Y poses an interesting problem. During thermal regeneration of H-Y, the $Fe(CO)_5$ concentration in the effluent stream raises significantly. Therefore, the thermal regeneration effluent will have high concentrations of $Fe(CO)_5$ at given points. This poses an obvious safety concern. The thermal regeneration effluent is an extremely toxic off-gas that must be dealt with safely, i.e., thermal decomposition of the species may be the best practice.

In addition, a further safety concern is that thermal regeneration of $Fe(CO)_5$ laden adsorbents leads to deposition of elemental iron on the adsorbent. It is well known that supported, finely divided, metallic species are pyrophoric. Thus, when TSA beds are to be replaced, the possible pyrophoric nature of the "spent" adsorbent must be taken into consideration. This pyrophoric property is particularly a concern with respect to finely divided metallic species present on carbonaceous surfaces.

Effect of Carrier Gas Pressure on $Fe(CO)_5$ Adsorption

It is important to investigate the effect of pressure on trace impurity removal. As the pressure of the carrier gas increases, the adsorption capacity for trace impurity decreases. This is because at higher adsorption

pressures the competition for adsorption sites between the trace impurity and the bulk carrier is enhanced. Thus, the much more prevelant carrier gas molecules inhibit the adsorption of the trace impurity.

Figure 12 depicts $Fe(CO)_5$ adsorption isotherms on BPL carbon at 75°F from 40 psig (73% CO_2/26% N_2/1% CO) and 90 psig carrier (85% CO_2/14% N_2/1% CO). Clearly, the $Fe(CO)_5$ capacity is reduced when the carrier gas pressure is enhanced. At an equilibrium concentration of 5 ppm, the $Fe(CO)_5$ capacity drops from 0.96 to 0.62 mmole/g as the carrier gas pressure increases from 40 to 90 psig.

Figure 13 shows $Fe(CO)_5$ adsorption isotherms on H-Y zeolite at 75°F from 40 psig carrier (73% CO_2/26% N_2/1% CO) and 90 psig carrier (85% CO_2/14% N_2/1% CO). Once again, as in the case of adsorption on BPL, at higher carrier gas pressure, the extent of adsorption is decreased.

Mixed Langmuir Prediction of $Fe(CO)_5$ Adsorption

Since coal gasifiers operate at pressures in excess of 90 psig, it is of interest to predict adsorption capacities at higher carrier gas pressures. Prediction of multicomponent equilibrium adsorption is a difficult and complex task. Perhaps the simplest method for predicting multicomponent equilibrium adsorption is to use a mixed Langmuir approach. The working equation for the single component Langmuir isotherm is given by:

$$n = \frac{mbP}{1+bP}$$

FIGURE 12

Effect of Gas Pressure on Fe(CO)5 Adsorption

75 F, BPL Carbon

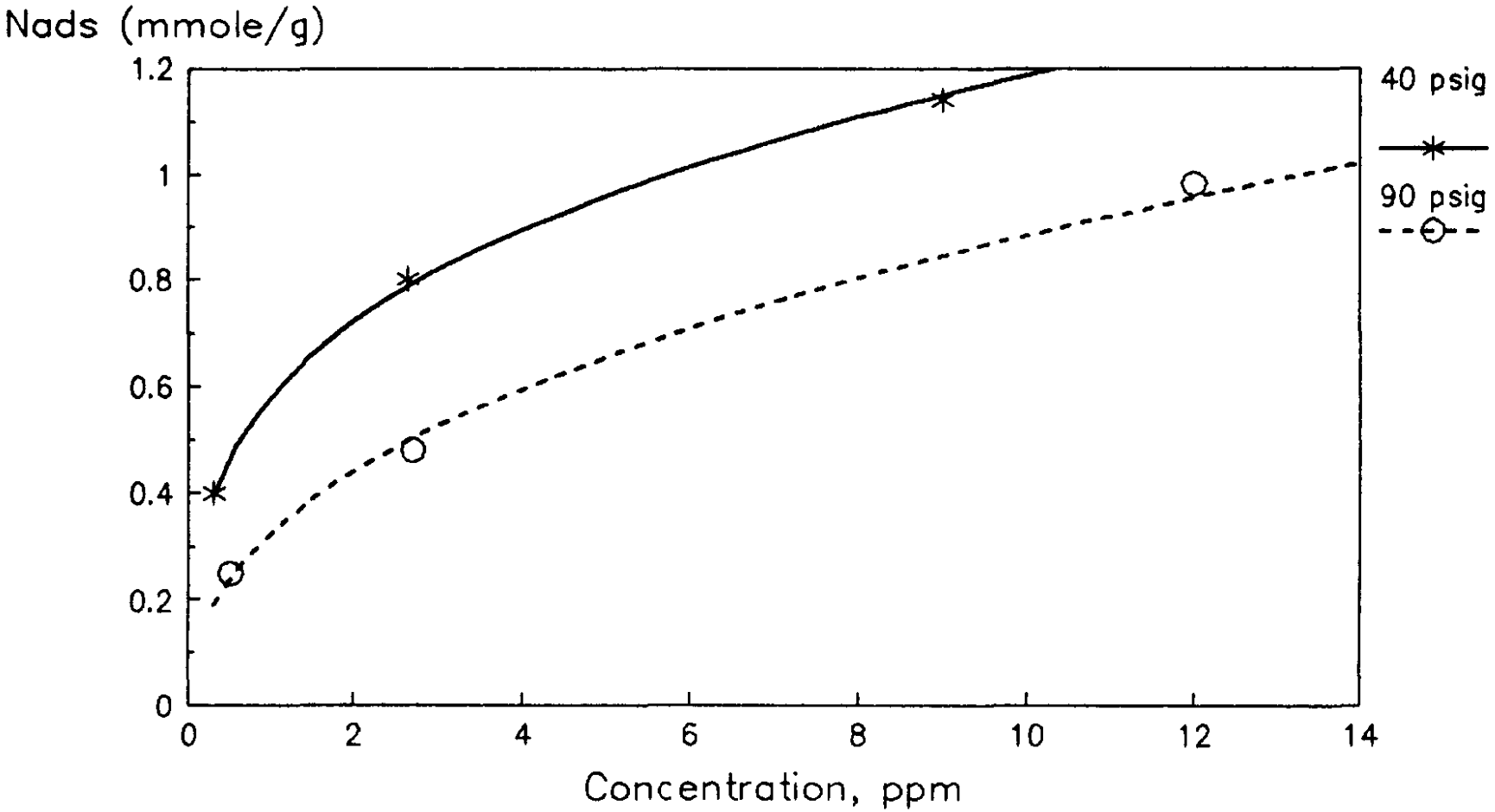

FIGURE 13

Effect of Gas Pressure on Fe(CO)5 Adsorption

75 F, H-Y

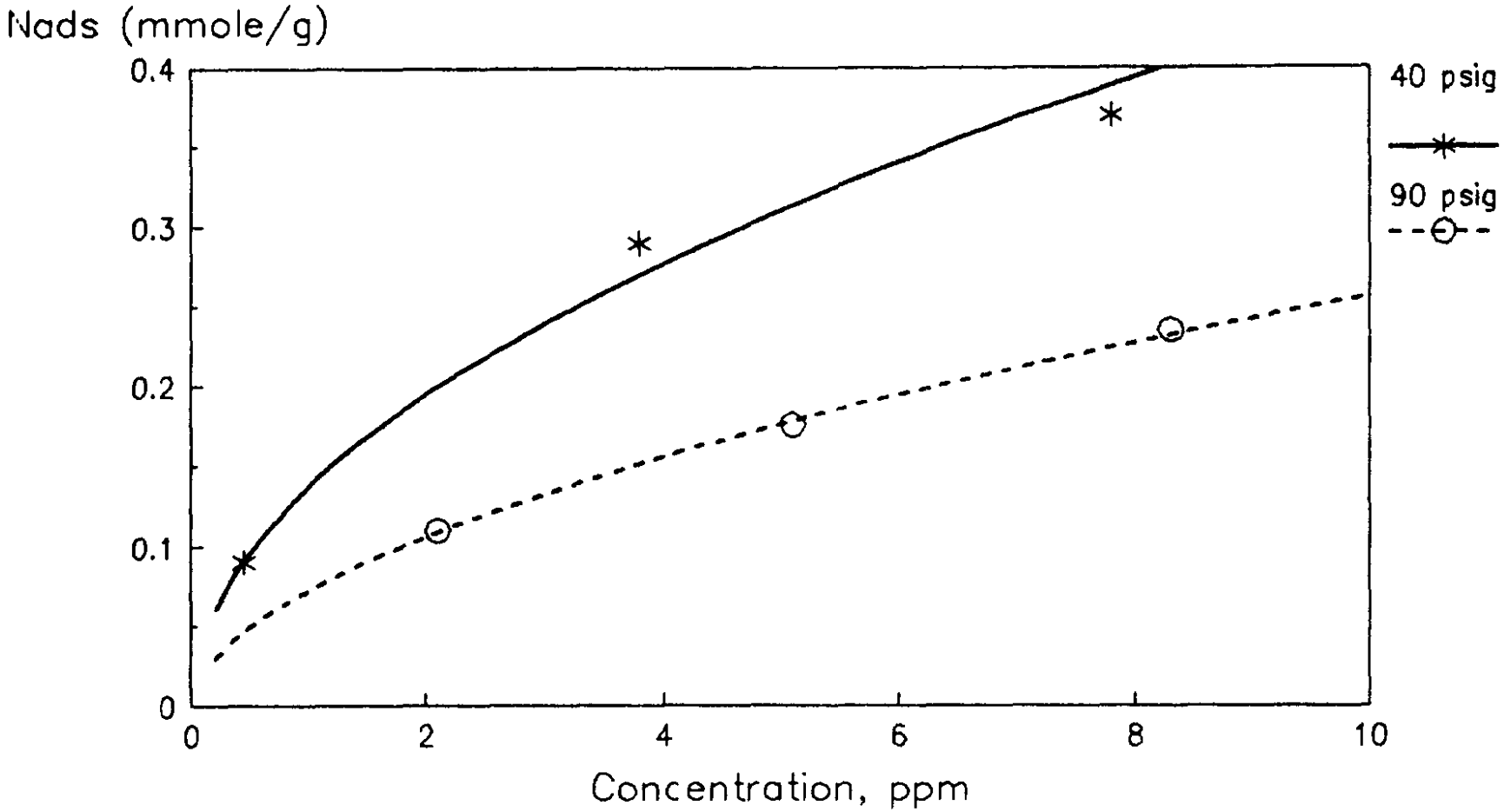

where n is the amount adsorbed, m is the monolayer capacity, b is an equilibrium adsorption coefficient, and P is the gas pressure. For the mixed Langmuir equation, the working equation is:

$$n = \frac{mbP}{1+\Sigma bP}$$

wherein the denominator of the equation is the summation of the bP products for each component in the multicomponent mixture. Thus, to predict the amount adsorbed of a given component in a multicomponent mixture one has to know a monolayer capacity, the equilibrium adsorption coefficient for each components (obtained from single component isotherms) and the partial pressure of each component in the gas mixture.

The mixed Langmuir technique was used to predict $Fe(CO)_5$ adsorption on Linde H-Y zeolite at 75°F from 90 psig carrier (85% CO_2/14% CO/1% N_2). The equilibrium adsorption coefficients for CO_2, CO, and N_2 were obtained from pure component isotherms and that for $Fe(CO)_5$ was obtained from 40 psig carrier data. Figure 14 shows the adsorption isotherms predicted by the mixed Langmuir technique and the actual experimental data. The results in Figure 14 show that the mixed Langmuir underpredicts by about 40% the amount of $Fe(CO)_5$ adsorption. At an equilibrium concentration of 5 ppm under the given conditions, the amount of $Fe(CO)_5$ adsorbed is 0.18 mmole/g vs. 0.13 mmole/g predicted by mixed Langmuir. Thus, mixed Langmuir does a reasonable job of predicting the effect of carrier gas pressure on $Fe(CO)_5$ adsorption. The theoretical value is less than the experimental value suggesting that use of the theory will provide a conservative estimate of adsorption capacity.

FIGURE 14

Mixed Langmuir Prediction of Fe(CO)5 Adsorption

75 F, 90 psig on H-Y

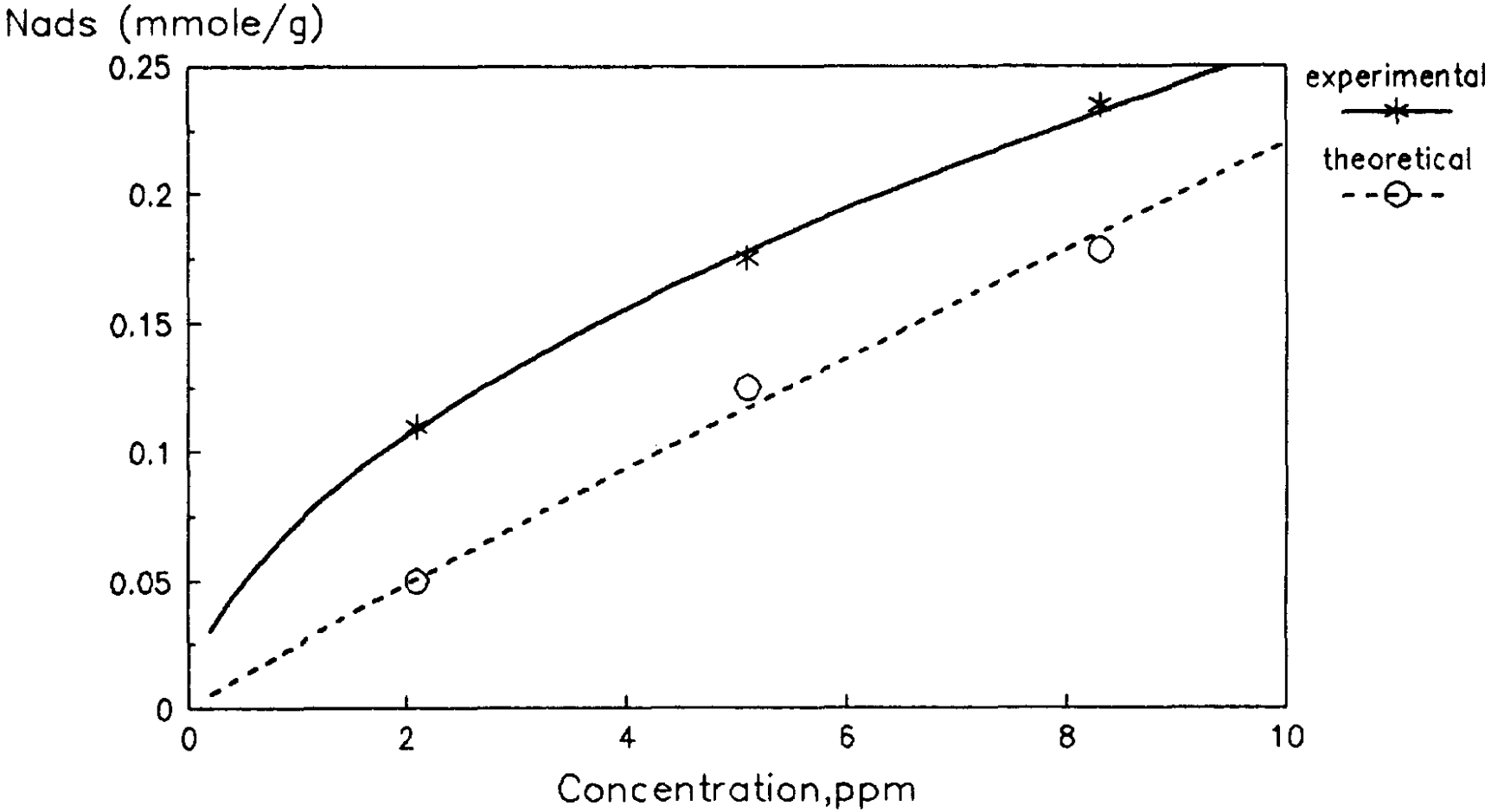

Adsorbent Selection for $Fe(CO)_5$ Adsorption

Of the adsorbents screened for $Fe(CO)_5$ removal, BPL carbon and H-Y zeolite are both useful adsorbents. At 90 psig (85% CO_2/14% CO/1% N_2) and 5 ppm, the capacities of BPL carbon and H-Y zeolite are 0.62 and 0.18 mmole/g, respectively. Thus, activated carbon has more than three times the capacity of zeolite. However, zeolite has a number of advantages over carbon. First, regeneration experiments indicate that the capacity of activated carbon is reduced on thermal cycling, which is not the case for zeolite. Second, zeolite has a 40% larger bulk density than carbon. Finally, thermal regeneration of $Fe(CO)_5$ laden adsorbents may produce a pyrophoric material. This may prove to be more of a problem with carbonaceous adsorbents than with inorganic ones.

Adsorption of $Ni(CO)_4$

Adsorbents Screened

Due to the carcinogenic nature of $Ni(CO)_4$, the total number of experiments done with this adsorbate was kept to a minimum. Based on the results obtained with $Fe(CO)_5$, adsorption isotherms were measured for $Ni(CO)_4$ with BPL carbon and H-Y zeolite only.

Figure 15 shows $Ni(CO)_4$ adsorption isotherms on BPL carbon and H-Y zeolite at 75°F from 40 psig carrier (95% N_2, 5% CO). The capacities at an equilibrium concentration of 1 ppm $Ni(CO)_4$ for BPL and H-Y are 0.22 and 0.07 mmole/g, respectively. The corresponding values for $Fe(CO)_5$ adsorption

FIGURE 15

Ni(CO)4 Adsorption on BPL and H-Y

75 F and 40 psig

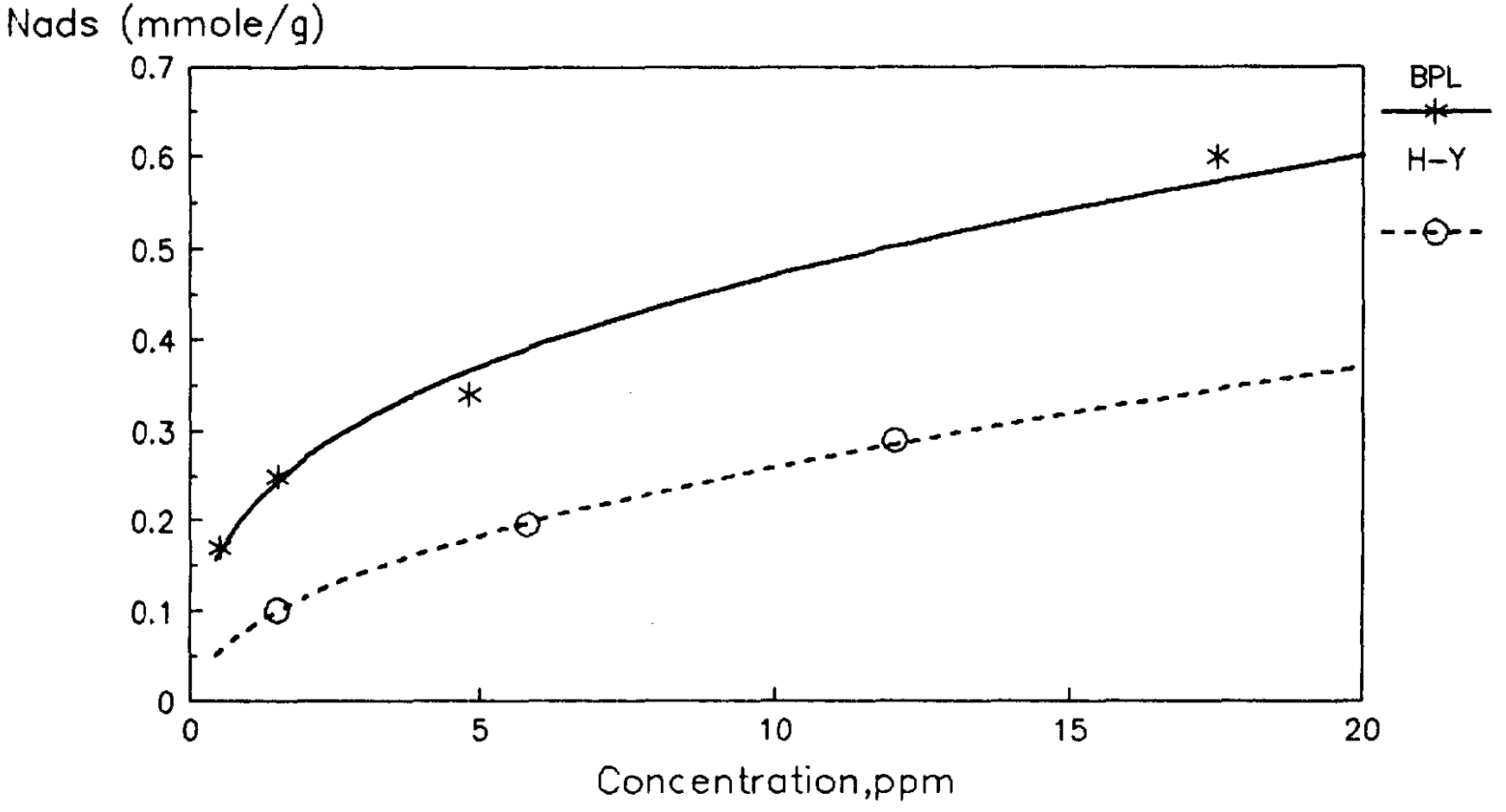

under the same conditions are 0.60 and 0.24 mmole/g. Thus, $Ni(CO)_4$ is adsorbed less strongly on these adsorbents than $Fe(CO)_5$ which is expected from the lower molar volume and higher saturation vapor pressure of $Ni(CO)_4$.

The Effect of Temperature on $Ni(CO)_4$ Adsorption

The effect of temperature on $Ni(CO)_4$ adsorption was investigated. Figure 16 shows $Ni(CO)_4$ adsorption isotherms on Linde H-Y from 40 psig carrier at 75 and 100°F. Figure 16 also gives the apparent heat of $Ni(CO)_4$ adsorption as a function of surface coverage. As was the case with $Fe(CO)_5$ adsorption, the magnitude of the heat of adsorption is large. At low surface coverage (0.05 mmole/g), the calculated heat of adsorption indicates a strong temperature dependence of $Ni(CO)_4$ adsorption. For example, the $Ni(CO)_4$ capacities at 1 ppm are 0.022 and 0.070 mmole/g at 100 and 75°F, respectively. Thus, the extent of $Ni(CO)_4$ adsorption can be largely affected by changing the adsorption temperature.

The effect of adsorption temperature on $Ni(CO)_4$ adsorption on BPL carbon was also investigated (Figure 17). As in all previous cases, the heat of adsorption is high and the decrease in heat as a function of surface coverage indicates adsorbent heterogenity. Clearly, reducing adsorption temperature provides an effective means of enhancing the adsorptive capacity of adsorbents for carbonyls.

FIGURE 16

Effect of Temperature on Ni(CO)4 Adsorption

40 psig on H-Y

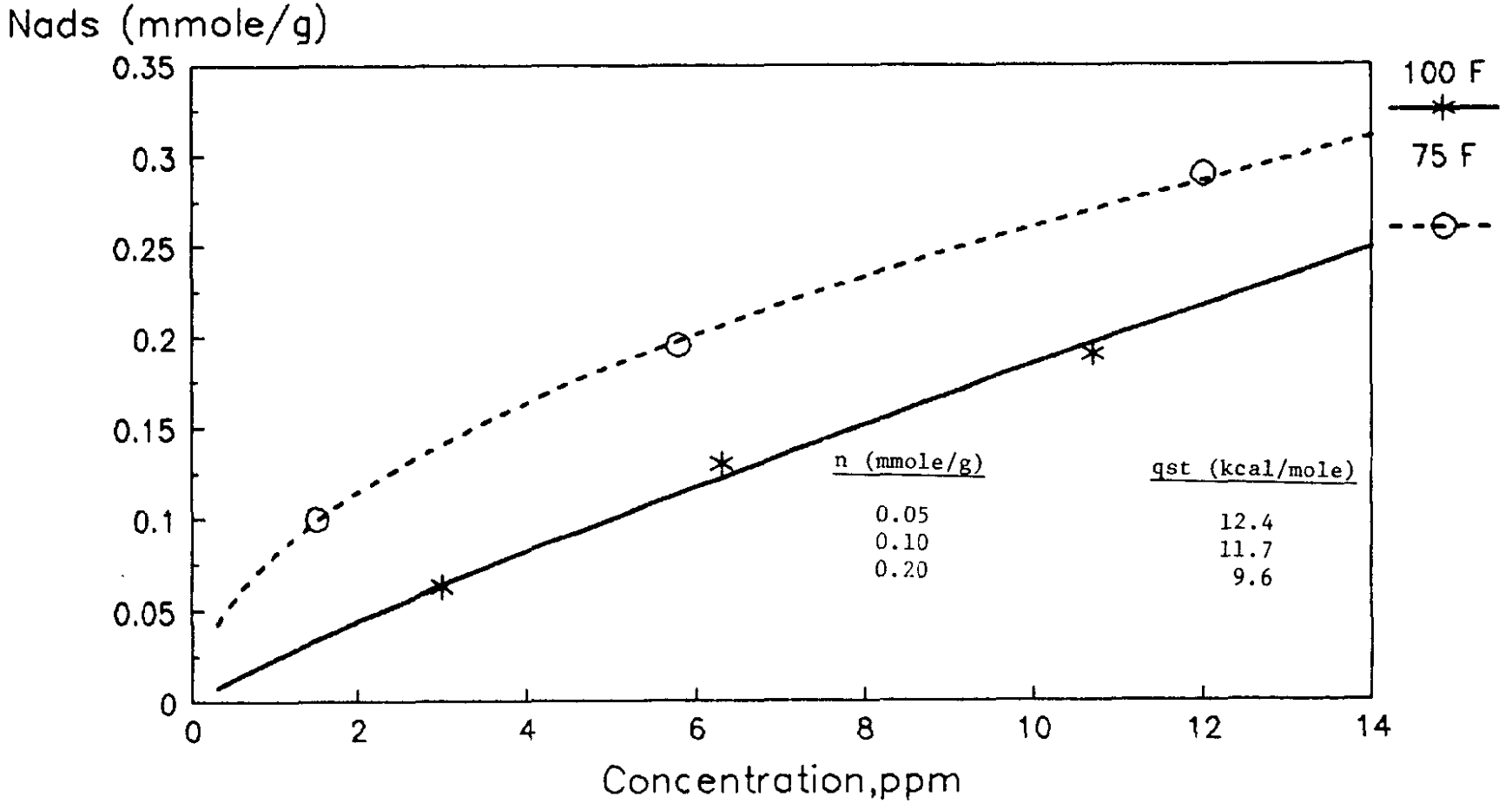

FIGURE 17

Effect of Temperature on Ni(CO)4 Adsorption

40 psig on BPL

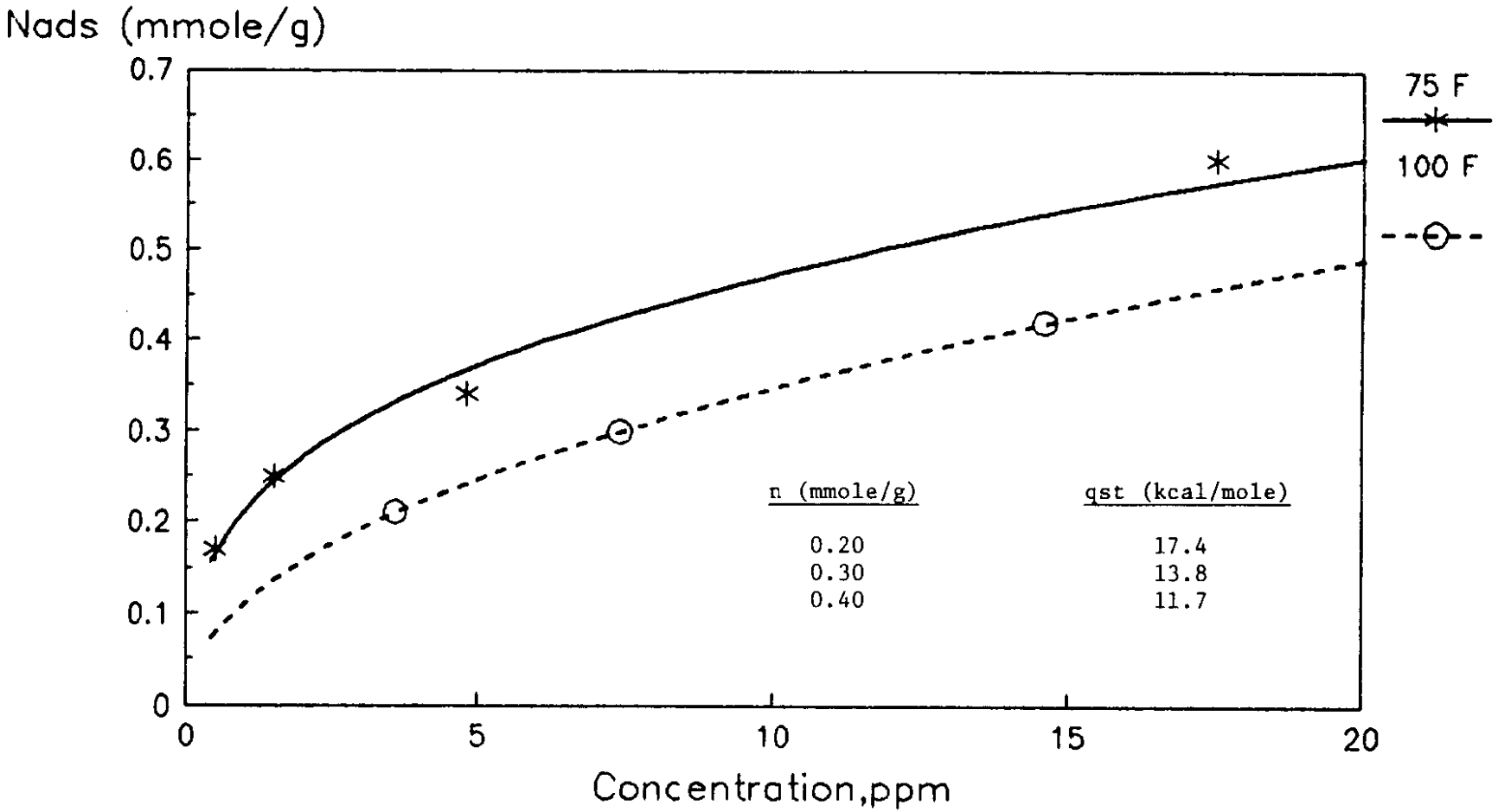

Effect of Carrier Gas Pressure on $Ni(CO)_4$ Adsorption

Figure 18 shows the effect of carrier gas pressure on the adsorption of $Ni(CO)_4$ on BPL carbon. As was the case with $Fe(CO)_5$ adsorption, higher carrier gas pressures decrease adsorption of the trace impurity. At 1 ppm $Ni(CO)_4$, the adsorption capacity of BPL carbon decreases from 0.20 to 0.05 mmole/g as the carrier gas pressure increases from 40 to 90 psig. This diminution is greater than that noted with $Fe(CO)_5$. This is to be expected since the effect of carrier gas pressure increases as the capacity for the trace impurity decreases. Thus $Fe(CO)_5$, which is adsorbed more strongly than $Ni(CO)_4$, is less affected by the carrier gas pressure.

Effect of Thermal Regeneration Studies on $Ni(CO)_4$ Adsorption

Figure 19 shows $Ni(CO)_4$ adsorption isotherms on BPL carbon at 75°F and 40 psig carrier (73% CO_2/26% N_2/1% CO) following three successive adsorption/regeneration cycles. Regeneration was carried out in N_2 at 250°F. As opposed to the $Fe(CO)_5$ adsorption/regeneration case, the $Ni(CO)_4$ capacity remains intact following these adsorption regeneration cycles. This is most probably due to the smaller capacity for $Ni(CO)_4$ than for $Fe(CO)_5$ demonstrated by BPL carbon.

Adsorbent Selection for $Ni(CO)_4$ Removal

The preferred adsorbent for $Ni(CO)_4$ removal is BPL activated carbon. The material demonstrates the highest $Ni(CO)_4$ adsorption capacity and is

FIGURE 18

Effect of Gas Pressure on Ni(CO)4 Adsorption

75 F on BPL

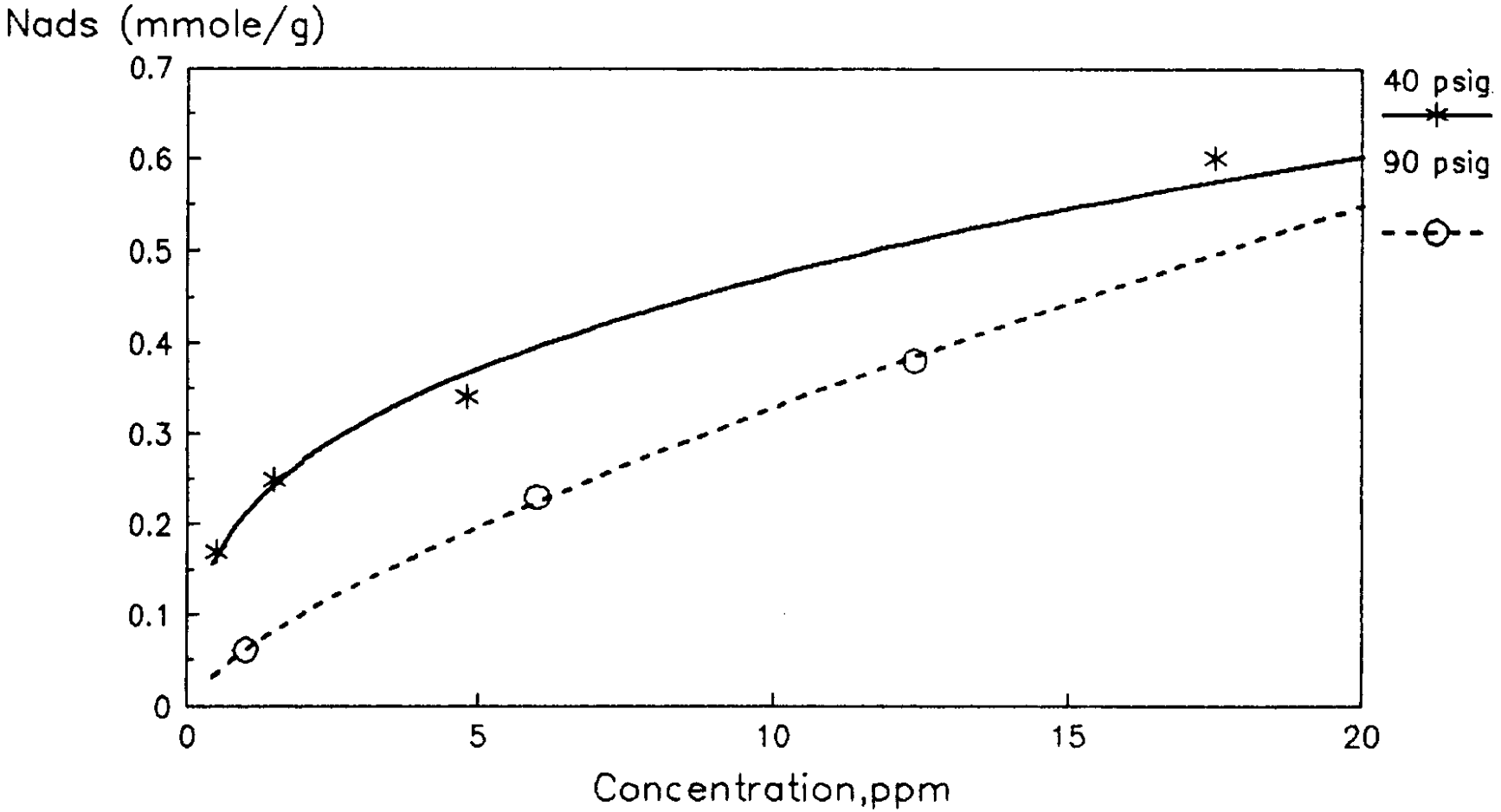

FIGURE 19

Effect of Regeneration on Ni(CO)4 Capacity

75 F and 40 psig on BPL

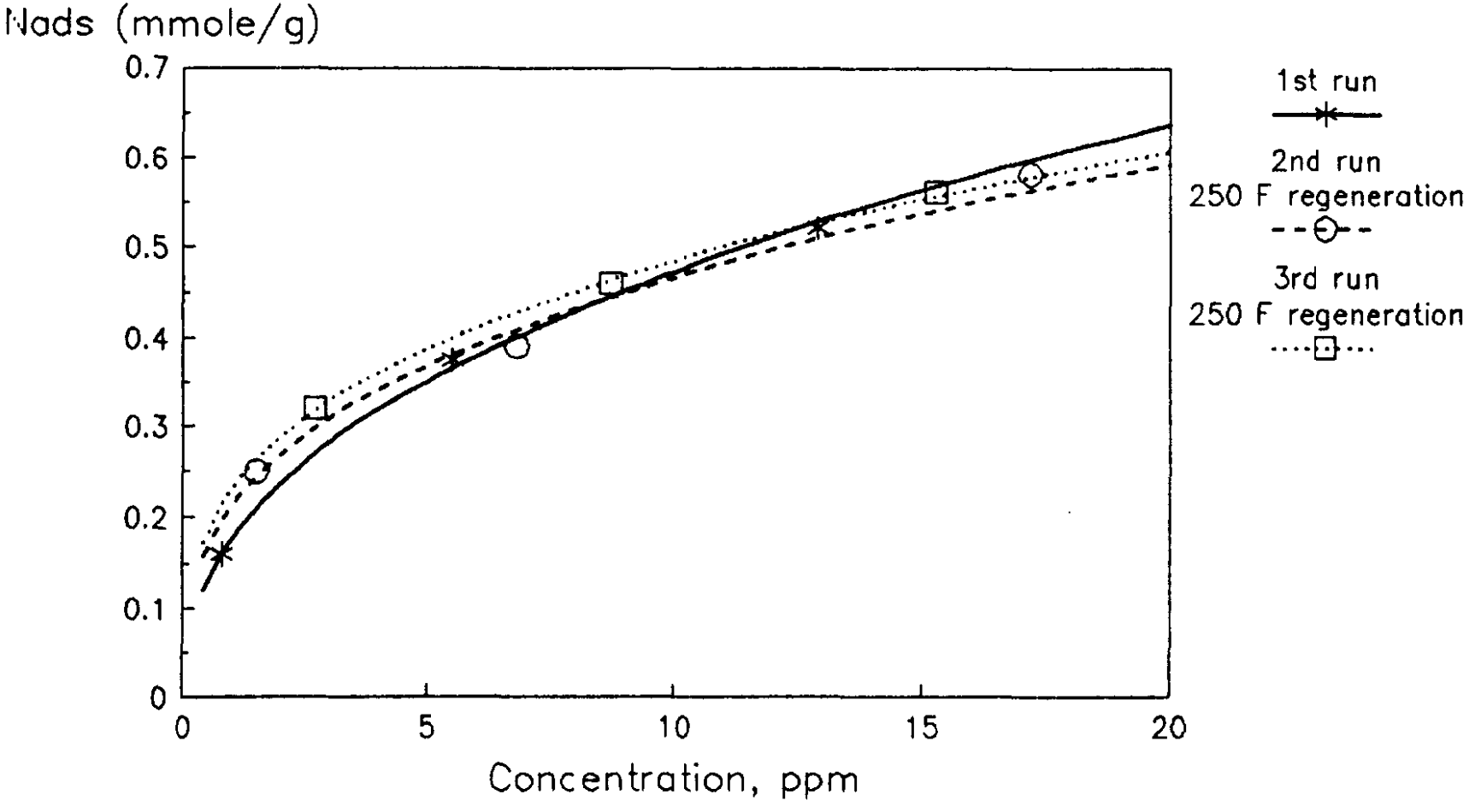

regenerable in N_2 at 250°F so that it should operate well in a conventional TSA system.

Adsorption of COS

Adsorbent Screening

Initial screening of adsorbents for COS removal was carried out by measuring adsorption isotherms at 75°F from 90 psig carrier gas (85% CO_2, 14% N_2, 1% CO). The adsorbents screened included a zeolite (Linde H-Y), an activated carbon (BPL carbon), a metal oxide promoted alumina (Alcoa Selexsorb COS), a metal oxide promoted zinc oxide (UCI-C125-1-01), an iron oxide impregnated activated carbon (Barneby-Cheney type CJ), a sodium oxide impregnated carbon (10% Na_2O on BPL), a copper oxide/chromium oxide impregnated carbon (Calgon type FCA), and a spent methanol catalyst (ICI EPJ-19).

The results of adsorbent screening are shown in Figure 20. First, only type FCA carbon shows appreciable adsorption capacity for COS. The adsorption capacities of H-Y and BPL carbon at an equilibrium concentration of 10 ppm are ~2 X 10^{-3} mmole/g. Clearly, this capacity is quite low. In addition, the capacities of sodium oxide and iron oxide impregnated carbon as well as promoted alumina and zinc oxide are lower than that for zeolite and activated carbon. Second, spent MeOH catalyst, EPJ-19, demonstrates the second highest COS capacity. Thus, those adsorbents screened with high COS capacity, EPJ-19 and FCA, both contain copper.

FIGURE 20

COS Adsorption on Various Adsorbents
75 F and 90 psig

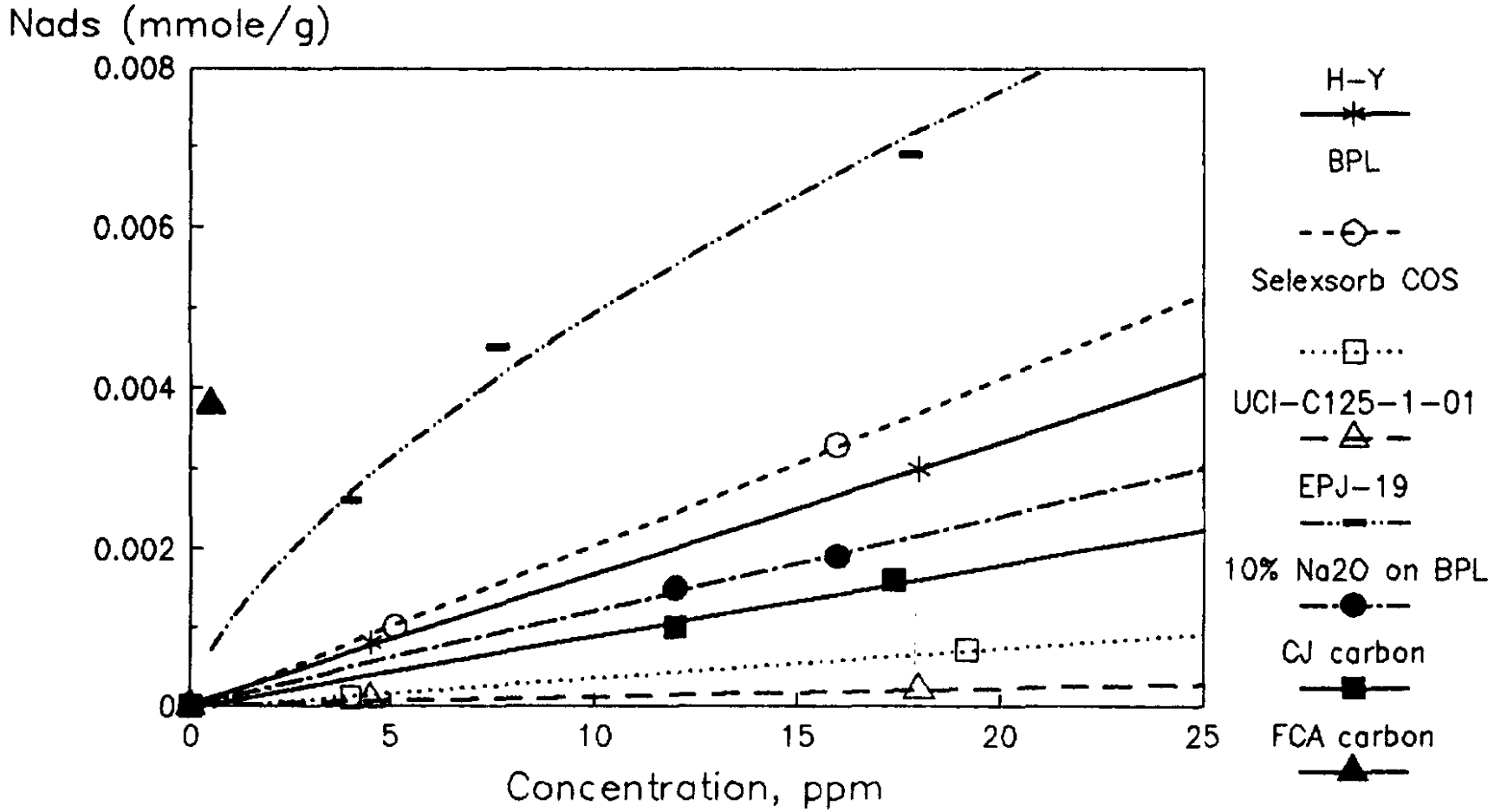

Effect of Regeneration on COS Adsorption on FCA Carbon

Since FCA carbon displayed the highest COS capacity of all adsorbents screened, the ability to regenerate the adsorbent was investigated. Figure 21 shows successive COS adsorption isotherms at 75°F and 90 psig carrier (85% CO_2, 14% CO, 1% N_2) on FCA carbon following various regeneration conditions. A freshly regenerated FCA sample showed a COS capacity of 0.067 mmole/g at an equilibrium concentration of 10 ppm. The "spent" adsorbent was then regenerated in N_2 at 250°F for 16 hours. The resulting COS capacity at 10 ppm dropped to 0.028 mmole/g indicating that this regeneration condition did not totally recover the COS capacity. To test the effect of regeneration gas, the sample was then regenerated for 16 hours at 250°F in CO_2. Again, the COS capacity was less than the original, indicating that the regeneration gas had no effect on the ability to regenerate the COS capacity. Finally, the effect of regeneration temperature was investigated and the sample was regenerated in N_2 at 500°F in N_2 for 16 hours. This treatment recovered the initial COS capacity. Subsequently, the adsorbent was regenerated again at 500°F in N_2 to ensure that the capacity remains intact following an adsorption/regeneration cycle at 500°F. After this second regeneration at 500°F, the COS capacity remained constant. Thus, type FCA carbon is a reversible COS adsorbent with regeneration at 500°F in N_2.

Effect of Temperature on COS Adsorption

The adsorption of COS on fresh type FCA carbon was carried out at 100°F so that the apparent isosteric heat of COS adsorption could be calculated.

FIGURE 21

Effect of Regeneration on COS Capacity

75 F and 90 psig on FCA carbon

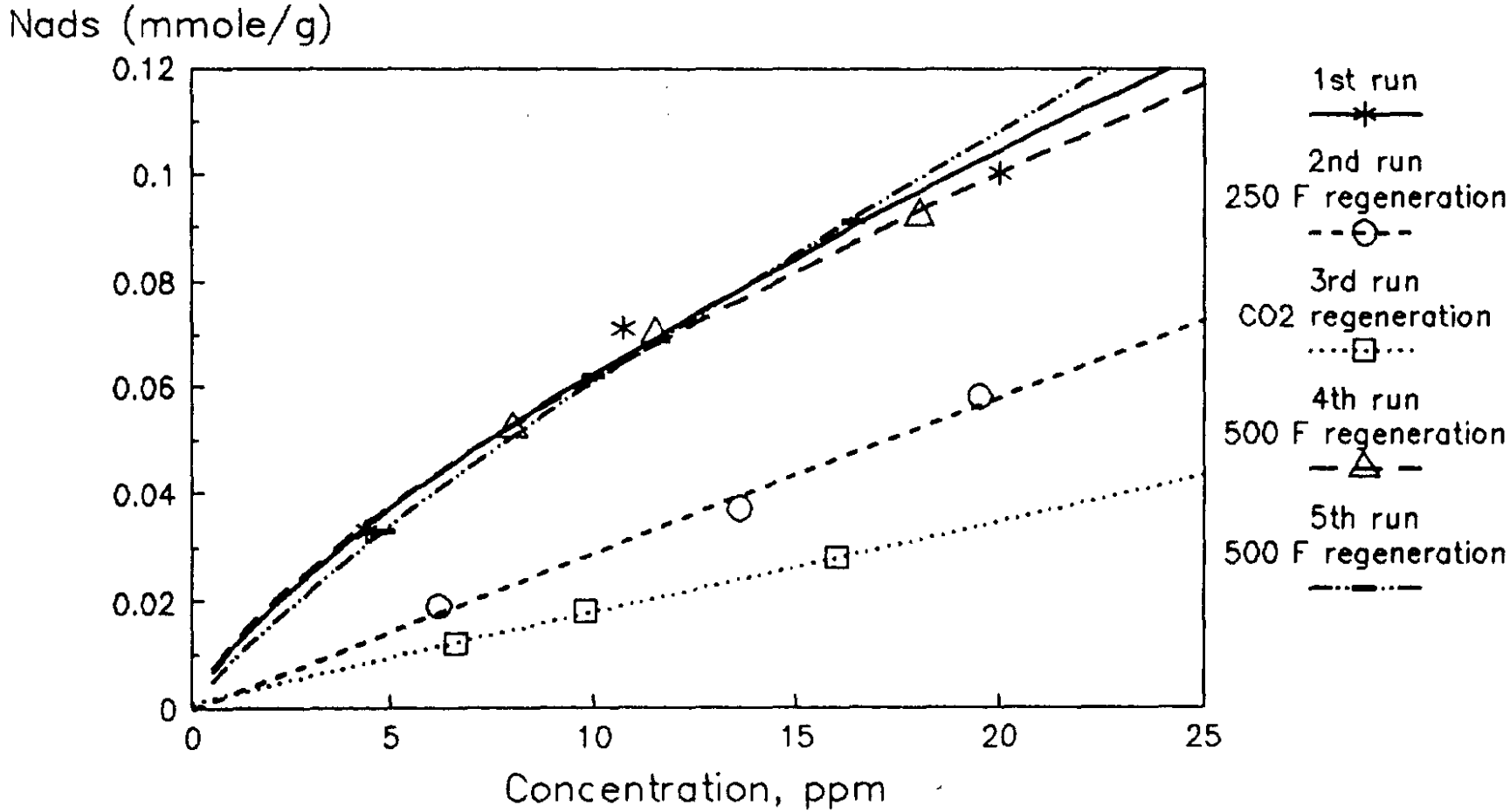

Figure 22 shows trace COS isotherms at 75 and 100°F. Also shown is the apparent heat of COS adsorption as a function of surface coverage. The apparent heat of adsorption at low surface coverage (0.01 mmole/g) is 13.1 kcal/mole; this value drops to 10.9 kcal/mole at 0.04 mmole/g indicating some adsorbent heterogenity. Furthermore, this relatively high heat of adsorption suggests that adsorption capacity can be significantly enhanced by reducing the adsorption temperature.

Adsorbent Selection for COS Removal

Of all the adsorbents screened, the preferred adsorbent for COS removal by adsorption at ambient temperatures is Calgon type FCA carbon. This adsorbent can be used in a regenerable temperature swing adsorption system with regeneration occurring at 500°F.

Adsorption of H_2S

Adsorbent Screening

Initial screening of adsorbents for H_2S removal was done by measuring trace H_2S adsorption isotherms at 75°F from 90 psig carrier gas (85% CO_2, 14% CO, 1% N_2). The adsorbents screened included two zeolites, Linde H-Y and Laporte CaX; BPL activated carbon; three impregnated active carbons, Calgon type FCA, desulf-8, and 10% (wt) MgO loaded BPL; two spent MeOH catalysts, EPJ-19 and BASF S3-85; and a promoted zinc oxide, Haldor-Topsoe, HTZ-4.

FIGURE 22

Effect of Temperature on COS Adsorption

90 psig on FCA carbon

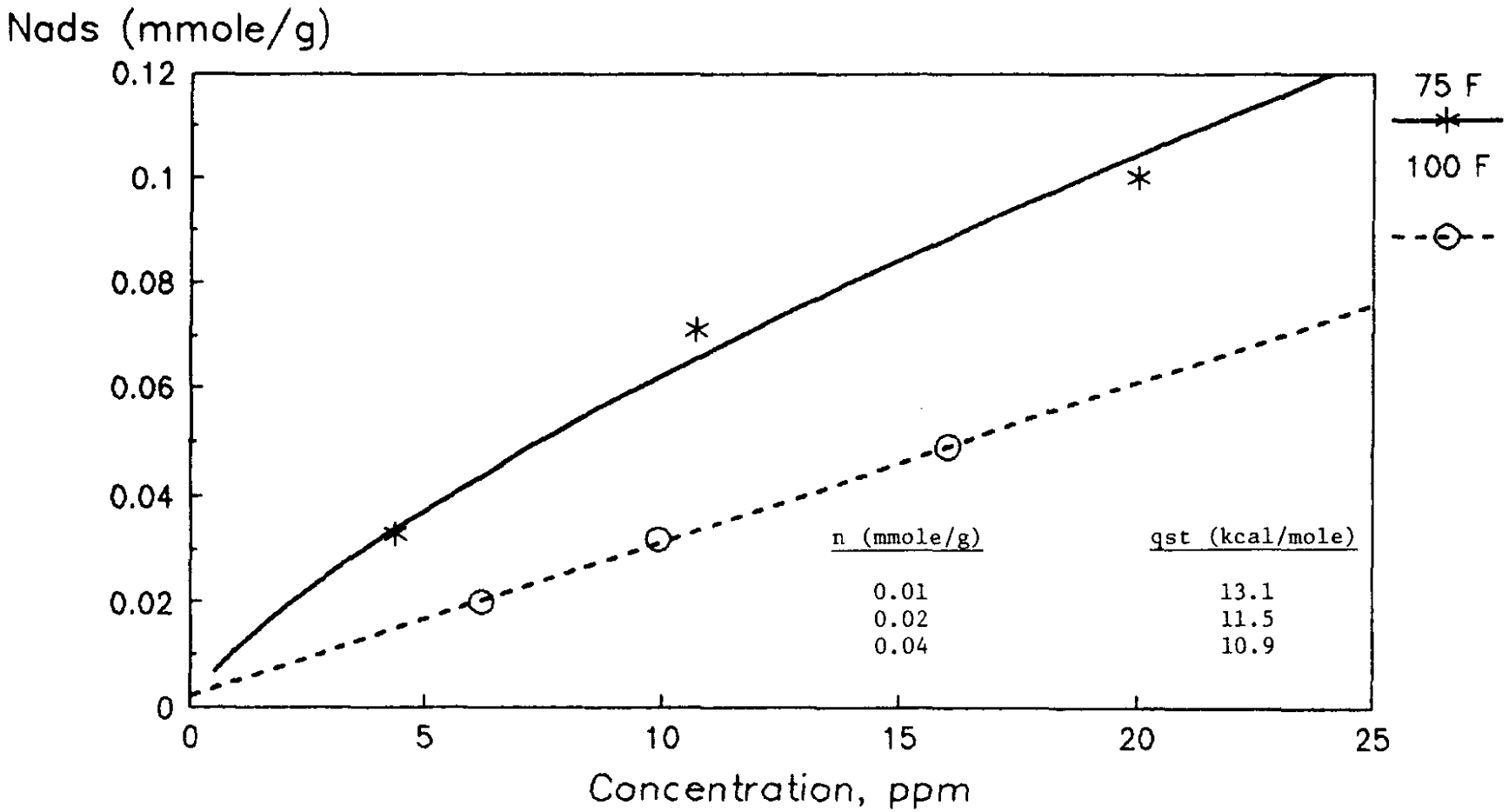

Figure 23 gives the H_2S adsorption isotherms on BPL, H-Y, CaX, HTZ-4, and 10% MgO on BPL. Interestingly, HTZ-4 shows significant H_2S capacity even at this low temperature, however, this capacity is not regenerable. Of the two zeolite adsorbents, H-Y yields a higher H_2S capacity than CaX. Even though H_2S is a polar adsorbate and CaX is a more polar adsorbent than H-Y, H-Y has a higher H_2S capacity under the conditions investigated. This is because the primary carrier gas, CO_2, is also a polar molecule which interacts more strongly with CaX than H-Y thereby reducing the capacity of CaX. Figure 23 also shows a comparison of H_2S adsorption on BPL carbon and 10% MgO on BPL carbon. The impregnation of a basic metal oxide like MgO on the surface of the carbon clearly increases the H_2S capacity. This can be explained as an acid-base interaction between MgO and acidic H_2S.

Figure 24 gives trace H_2S adsorption isotherms on the other adsorbents screened. These adsorbents all demonstrate enhanced H_2S capacity over the previous adsorbents. The highest H_2S capacities measured are for the two spent MeOH catalysts. BASF S3-85 shows the highest H_2S capacity (about 5 mmole/g at 2 ppm), which is about twice that of EPJ-19. The rectangular isotherm shape suggests a chemisorptive process occurs with these materials. The very high H_2S capacity of these spent catalysts indicate that they may be useful throw-away adsorbents. The H_2S capacities of the other two adsorbents, FCA and desulf-12, are lower than those for spent catalyst but still quite high. The H_2S capacity of FCA at 5 ppm is about 1.3 mmole/g and the corresponding value for desulf 12 is about 0.7 mmole/g. The advantage of using these materials for H_2S removal is that they are both steam regenerable. Hence, these adsorbents could be employed in a steam regenerated TSA system for H_2S removal. One final point of interest is that all four

FIGURE 23

H2S Adsorption on Various Adsorbents
75 F and 90 psig

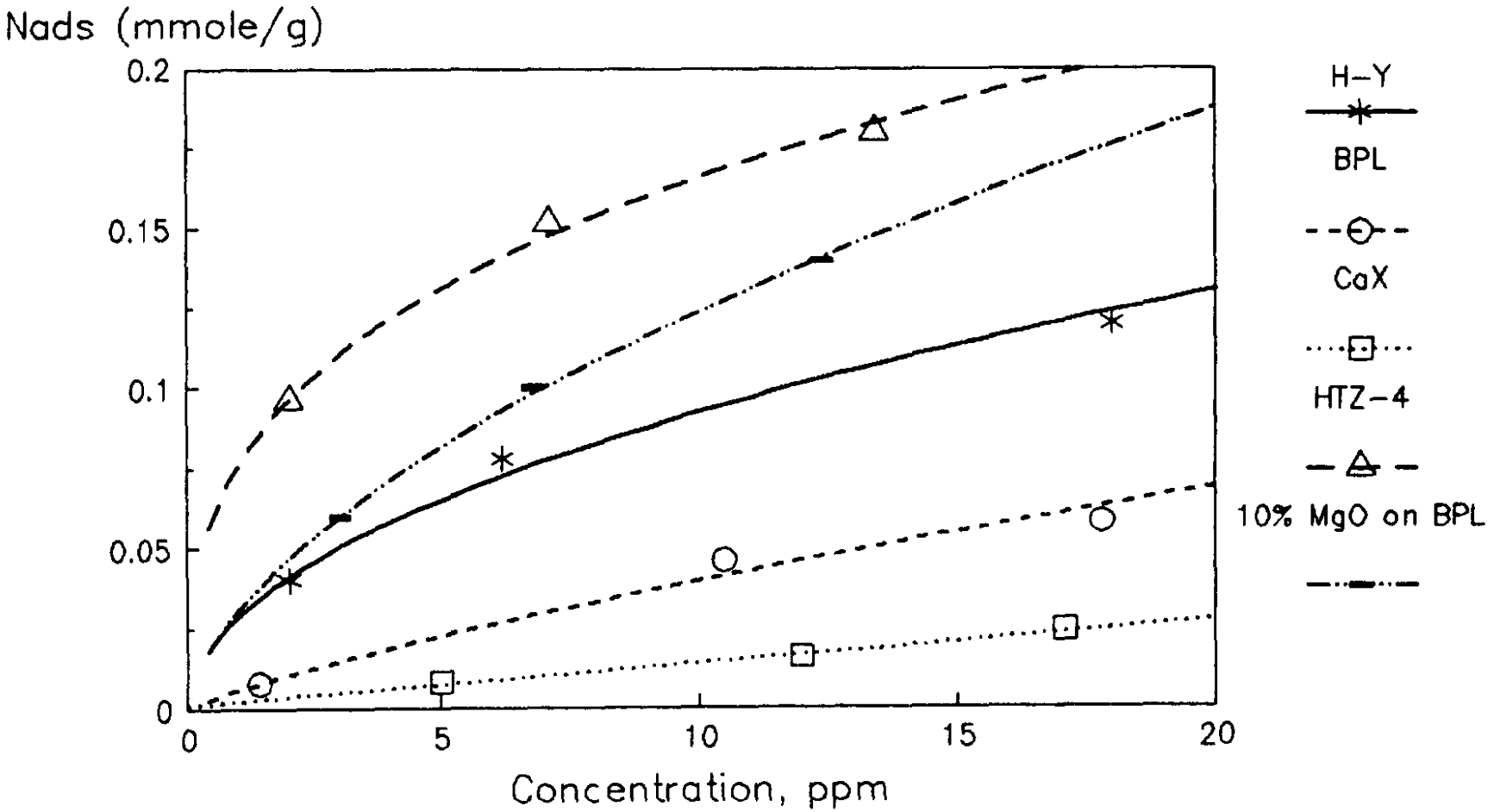

FIGURE 24

H2S Adsorption on Various Adsorbents
75 F and 90 psig

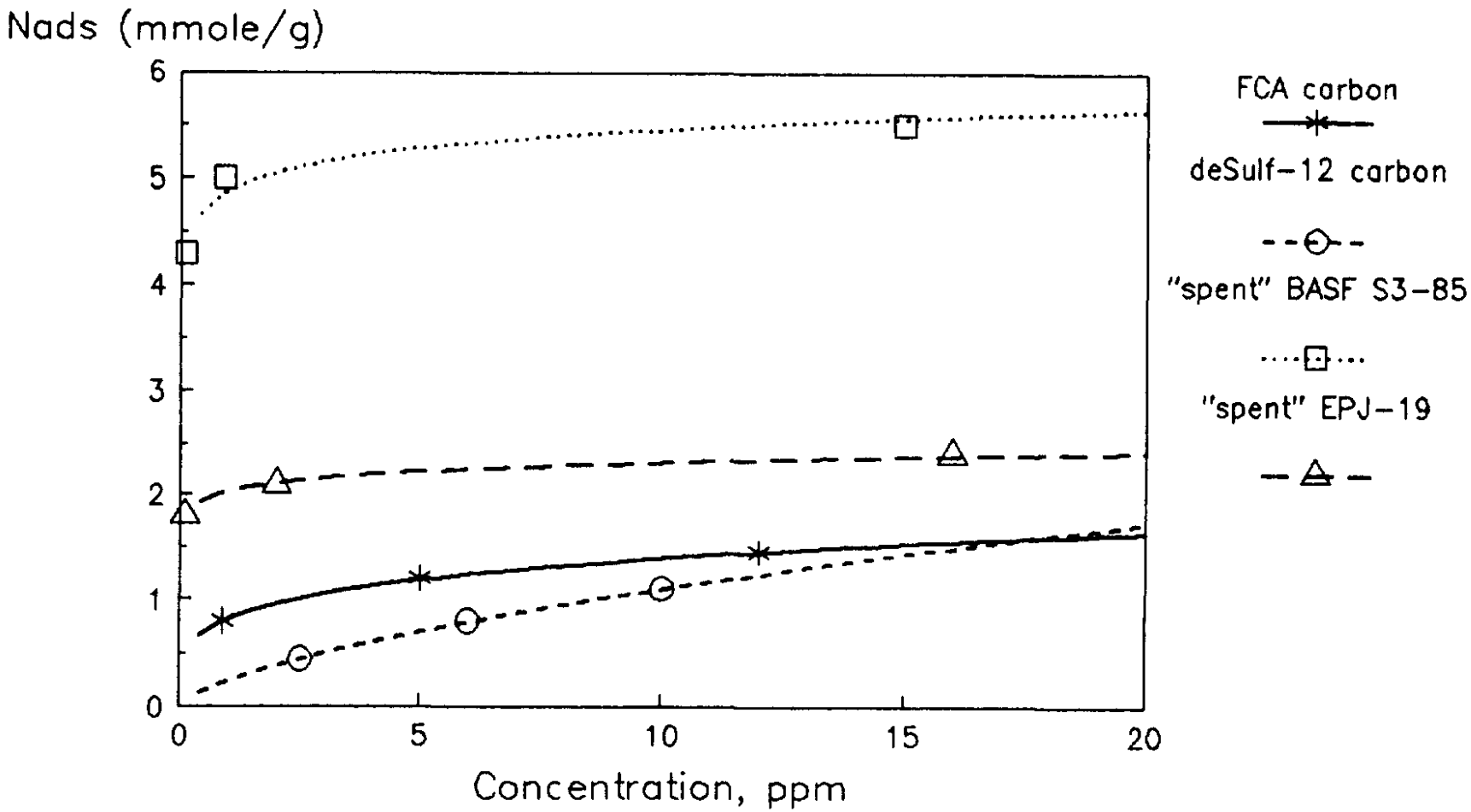

adsorbents shown in Figure 24 demonstrate high H_2S capacity and all contain copper. Thus, it may be expected that other copper containing materials, e.g., shift catalyst, will also have high H_2S capacities.

Another point to be made concerning H_2S removal using steam regenerable adsorbents like FCA carbon is that these materials are best suited for H_2S removal at low inlet H_2S concentrations. Looking at the isotherm for FCA in Figure 24 shows the H_2S capacity at 2 ppm is about equal to that at 10 ppm due to the rectangular isotherm shape. Thus, as the inlet H_2S concentration increases, the total H_2S needed to be processed increases, but the capacity remains relatively constant. Clearly, rectangular isotherm shapes are conducive to removing impurities at low inlet concentrations.

H_2S Adsorption on Linde H-Y Following $Fe(CO)_5$ Adsorption/Regeneration Cycles

From previous adsorption studies with $Fe(CO)_5$ it was determined that Linde H-Y may be a better adsorbent for $Fe(CO)_5$ removal than activated carbon, even though the initial capacity on carbon is greater than that on zeolite. This is because H-Y thermal regeneration is superior to carbon. However, thermal desorption curves and gravimetric analysis indicate that $Fe(CO)_5$ is decomposed during thermal regeneration leaving iron containing species on the adsorbent surface. The iron species may act as adsorption centers for sulfur containing gases, especially H_2S. To investigate this possibility, H_2S adsorption isotherms were measured on a sample of Linde H-Y that had gone through these adsorption/regeneration cycles with $Fe(CO)_5$. The iron weight loading on the adsorbent was 33%. Those adsorption isotherms are depicted in Figure 25.

FIGURE 25

H2S Adsorption on Fe(CO)5 laden H-Y

75 F and 90 psig

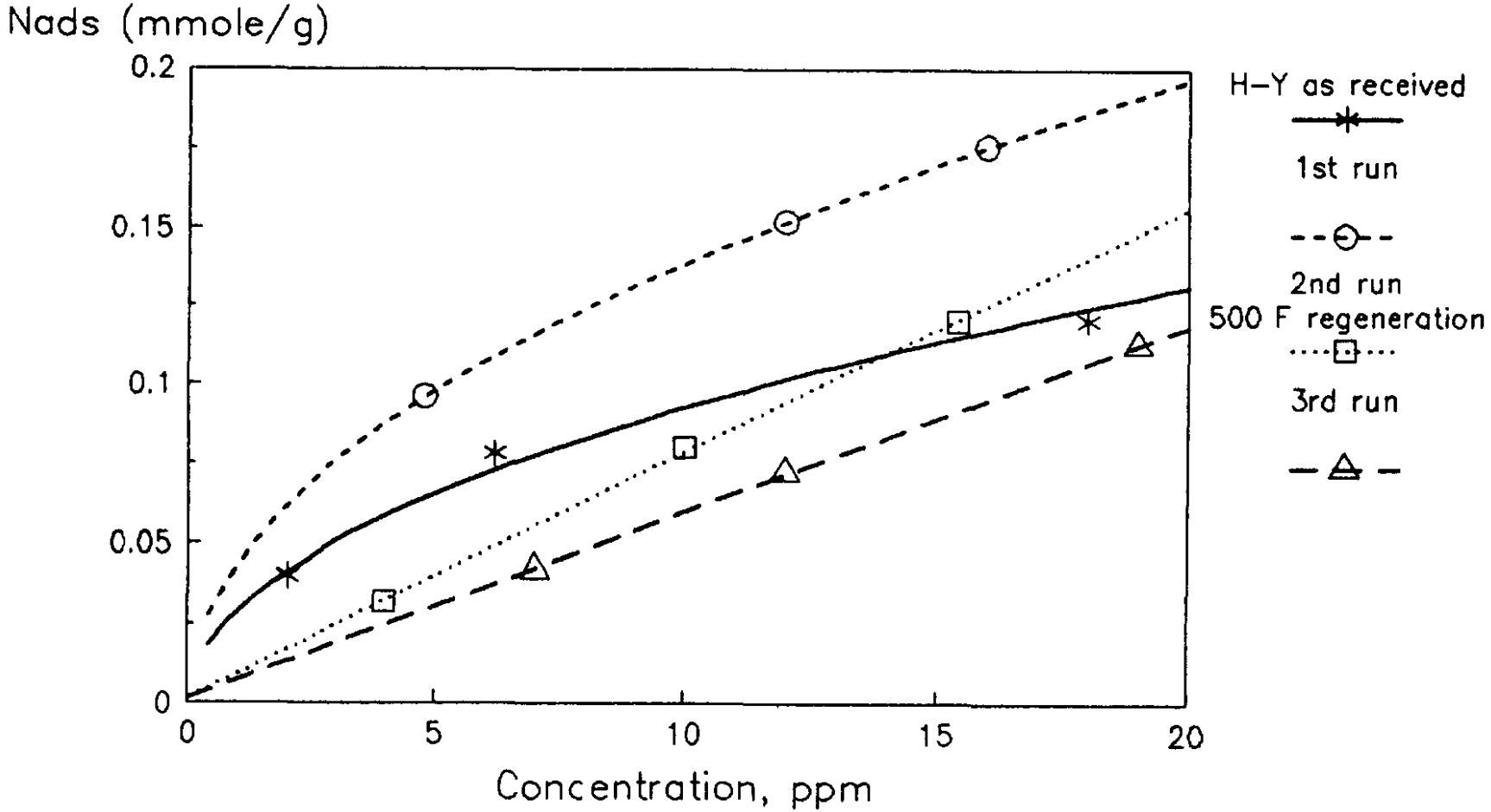

The figure shows a number of interesting points. First, the first H_2S isotherm on the iron contaminated zeolite shows a higher H_2S capacity than as-received H-Y. This suggests that deposited iron does act as an adsorption site for H_2S. Second, successive regenerations of this adsorbent at 500°F in N_2 following H_2S adsorption show a decrease in H_2S capacity. Presumably, the enhanced H_2S capacity noted in the first isotherm is due to chemisorption of H_2S, and this capacity is not recovered by thermal regeneration in N_2. These data indicate that the interaction between catalyst poisons on thermally regenerated adsorbents is a complex problem and must be considered during poison removal design.

Adsorbent Selection for H_2S Removal

The results from H_2S adsorption measurements indicate that a number of options for H_2S removal exist. Firstly, it appears that spent MeOH catalyst may provide a good throw-away adsorbent. Unfortunately, the form of the catalyst for LPMeOH production is powdered and a fixed bed adsorber requires some adsorbent with larger particle size. A liquid phase guard bed may, however, be useful. A second option is a regenerable system using type FCA carbon. Regeneration of FCA carbon requires 500°F steam since metallic sulfides from H_2S chemisorption must be reconverted to metallic oxides.

COS and H_2S Removal with Hot Zinc Oxide

Another conventional technology for COS and H_2S removal is hydrolysis of COS to H_2S and adsorption/reaction of H_2S on zinc oxide. To investigate this option for sulfur removal, COS hydrolysis and H_2S adsorption were measured

at 400°F on an alumina promoted zinc oxide (Haldor Topsoe HTZ-4). The H_2S capacity of HTZ-4 at 400°F from 90 psig CO_2 was determined to be 3.1 mmole/g or 10.5% by weight. This measured capacity agrees well with the vendor's reported capacity. In addition, the hydrolysis of COS with HTZ-4 was measured at 400°F and 90 psig CO_2 pressure. With an initial concentration of 156 ppm COS and 5000 ppm H_2O, the COS concentration was reduced to 1 ppm at equilibrium. The corresponding "capacity" was calculated to be 1.8 mmole/g.

Thus, hot promoted zinc oxide provides a viable sulfur removal system. The zinc oxide system provides a number of advantages over the ambient temperature adsorption approach. First, zinc oxide is a throw-away adsorbent so no regeneration system is needed. Second, this promoted zinc oxide works at significantly lower temperature than conventional zinc oxide. Finally, the COS capacity of HTZ-4 is significantly greater than any ambient temperature adsorbent.

It should be emphasized that only equilibrium information on COS and H_2S removal was obtained. Thus, the MTZ length for H_2S adsorption is still unknown.

Adsorption of HCl

Adsorbent Screening

Initial screening of adsorbents for HCl removal was carried out by measuring adsorption isotherms at 75°F from 90 psig carrier (85% CO_2, 14% N_2, 1% CO). The adsorbents screened included HY, BPL, Alcoa Selexsorb HCl,

Barneby-Cheney carbons type ST and CH, FCA carbon, and spent methanol catalyst, BASF S3-85.

Figure 26 shows adsorption isotherms on all adsorbents except S3-85. Type FCA carbon demonstrates the highest HCl capacity of those adsorbents depicted followed by type CH carbon. Thus, metal oxide loaded active carbons demonstrate high HCl capacity. The capacity of type FCA carbon at 5 ppm is 1.75 mmole/g or 6.4 wt%. The caustic impregnated carbon, type ST, demonstrates less HCl capacity than the metal oxide impregnated adsorbents. Perhaps unsurprising is that polar adsorbents like H-Y and selexsorb HCl adsorb more HCl than the non-polar active carbon, BPL. The HCl capacity of H-Y is a very respectable 0.40 mmole/g at 5 ppm.

Figure 27 gives the HCl isotherm on spent methanol catalyst BASF S3-85. The spent catalyst demonstrates very large HCl capacity, adsorbing 7.4 mmole/g at an equilibrium concentration of 5 ppm. This large capacity suggests that spent catalyst may be an acceptable throw-away adsorbent for HCl removal.

Effect of Thermal Regeneration on FCA Carbon and H-Y Zeolite

The effect of thermal regeneration on HCl capacity was investigated on type FCA carbon and H-Y zeolite. Figure 28 shows HCl adsorption isotherms at 75°F and 90 psig (85% CO_2/14% CO/1% N_2) on three successive adsorption/ regeneration cycles on FCA carbon. Regeneration was carried out in N_2 at 500°F. As noted, thermal regeneration in N_2 does not restore the HCl capacity of the adsorbent. This suggests that HCl is chemisorbed on FCA carbon. Thus, FCA cannot be used in TSA applications for HCl removal.

FIGURE 26

HCl Adsorption on Various Adsorbents
75 F and 90 psig

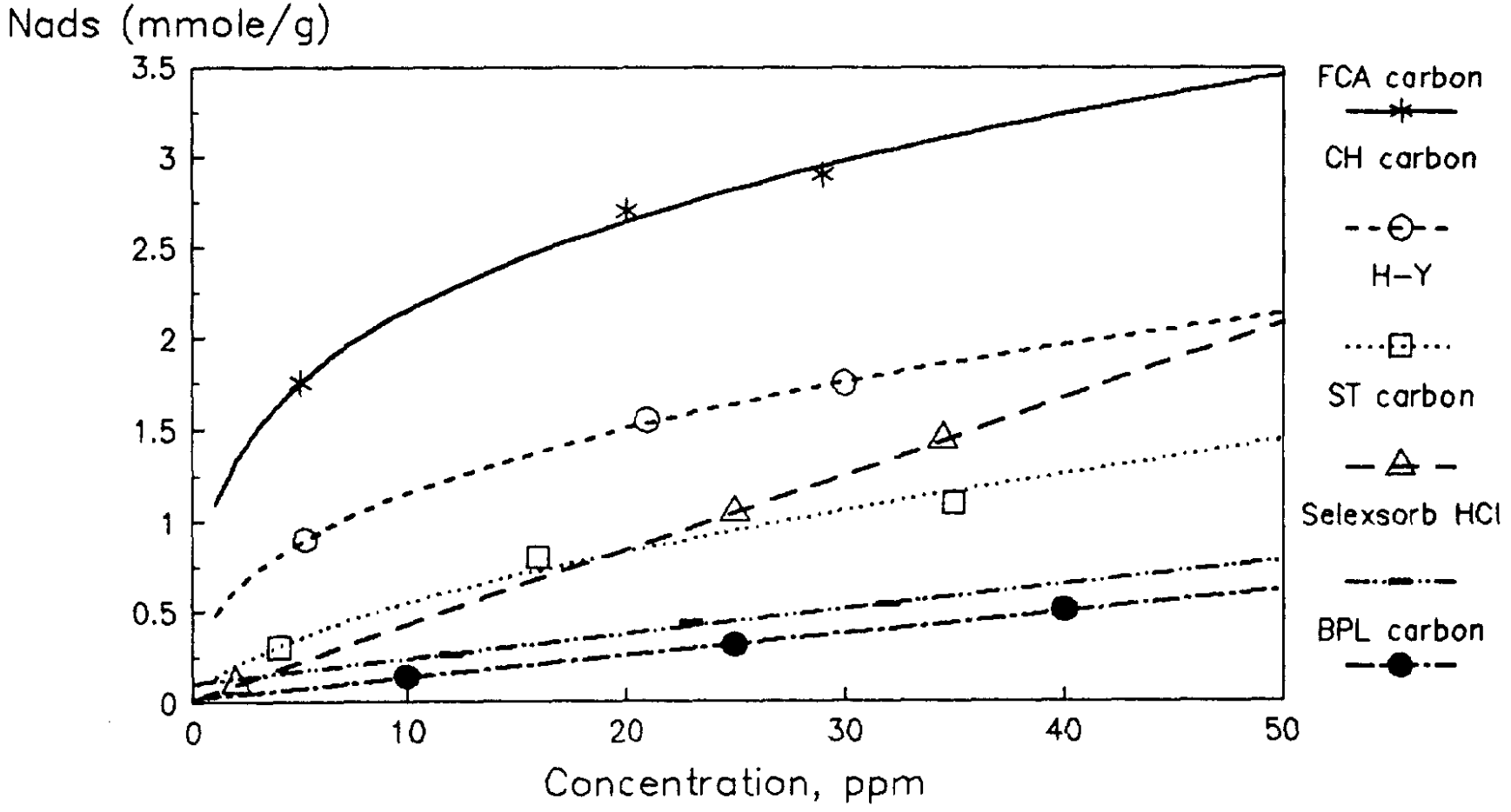

FIGURE 27

HCl Adsorption on BASF S3-85

75 F and 90 psig

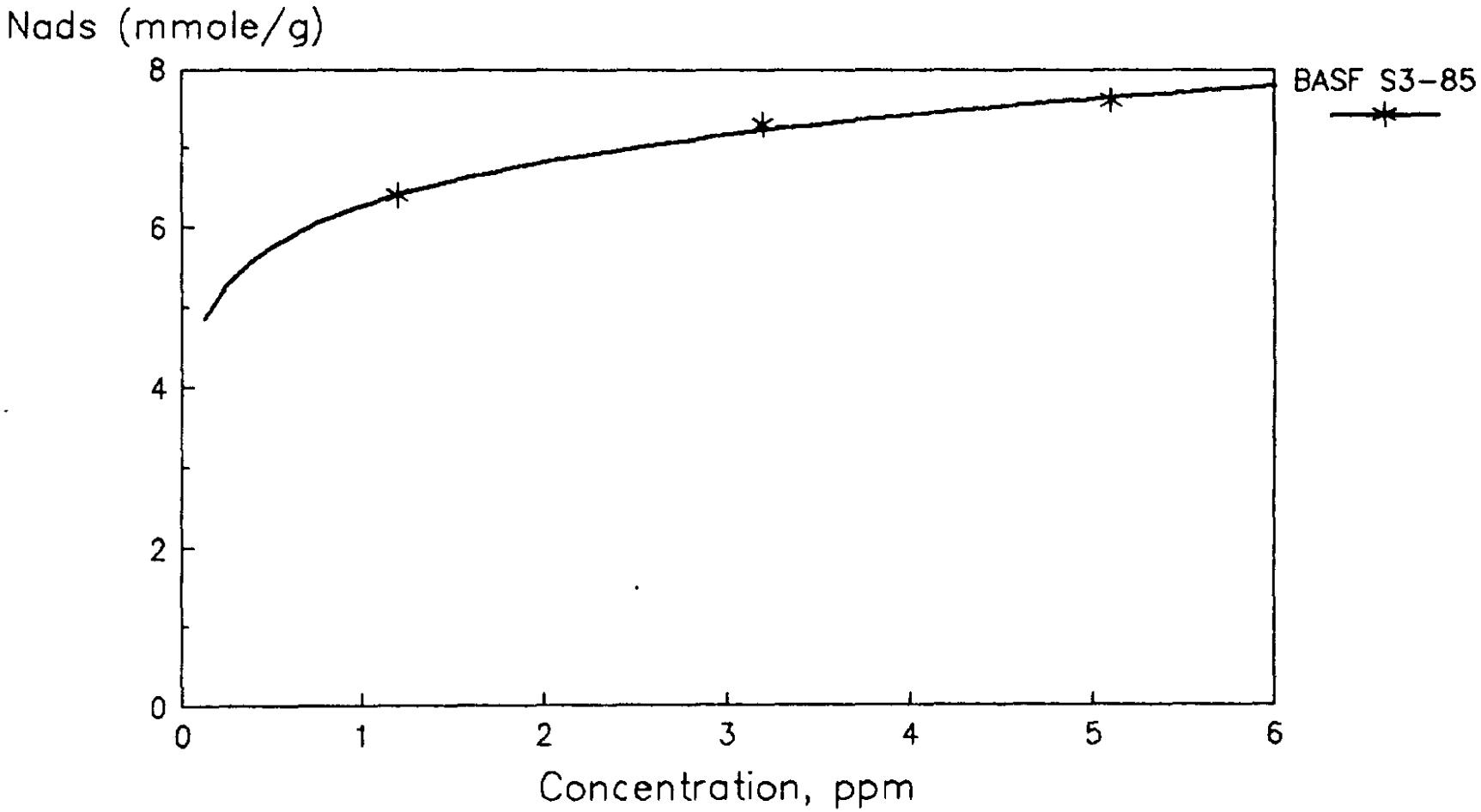

FIGURE 28

Effect of Thermal Regeneration on HCl Capacity

75 F and 90 psig on FCA carbon

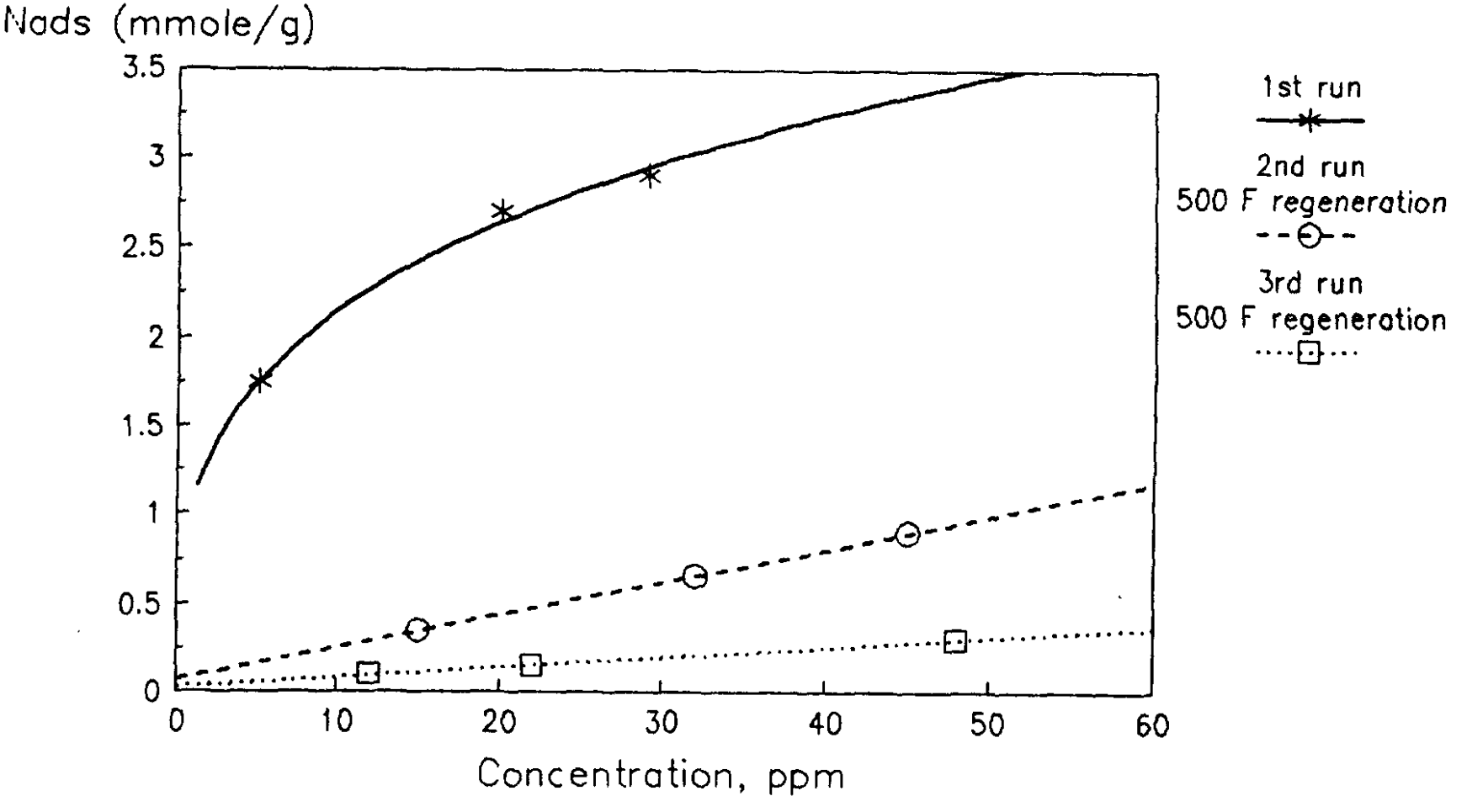

Figure 29 shows the HCl capacity on H-Y zeolite following two adsorption/regeneration cycles, regeneration carried out in N_2 at 500°F. As in the case with FCA carbon, thermal regeneration does not restore the initial HCl capacity. Once again, TSA removal of HCl with H-Y zeolite is not feasible.

Effect of Water Loading on HCl Capacity of H-Y Zeolite

Figure 30 shows HCl adsorption isotherms on Linde H-Y with two different water loadings. In general, as the water loading of a zeolite increases, its adsorptive capacity decreases because the water occupies available surface area and pore volume. However, since HCl is quite soluble in water, it was conjectured that the presence of water may in fact increase the HCl capacity. As noted in Figure 30, this is indeed the case. At an equilibrium concentration of 5 ppm, the sample with 0.0% water (regenerated in N_2 at 400°C) demonstrates an HCl capacity of 0.40 mmole/g, while the sample with 7.5% water has a capacity of 0.75 mmole/g. Hence, the presence of water on zeolite enhances its HCl capacity.

Adsorbent for HCl Removal

Of those adsorbents screened, the preferred adsorbent for HCl is spent methanol catalyst due to its large capacity. The large capacity, 7.4 mmole/g at 5 ppm, indicates that a throw-away adsorbent for HCl removal is a viable removal technique.

FIGURE 29

Effect of Thermal Regeneration on HCl Capacity

75 F and 90 psig on H-Y

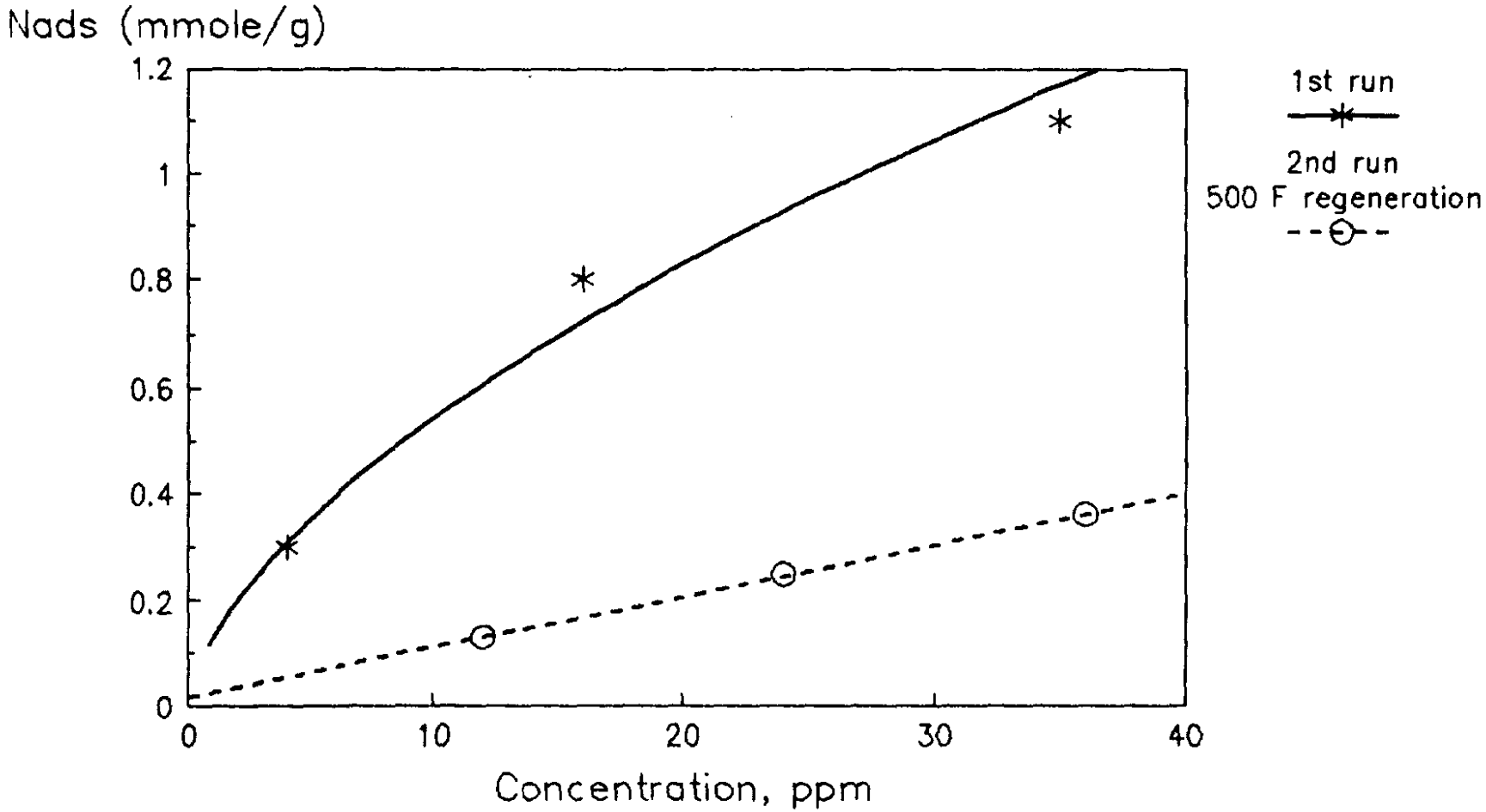

FIGURE 30

Effect of Water Content on HCl Capacity

75 F and 90 psig on H-Y

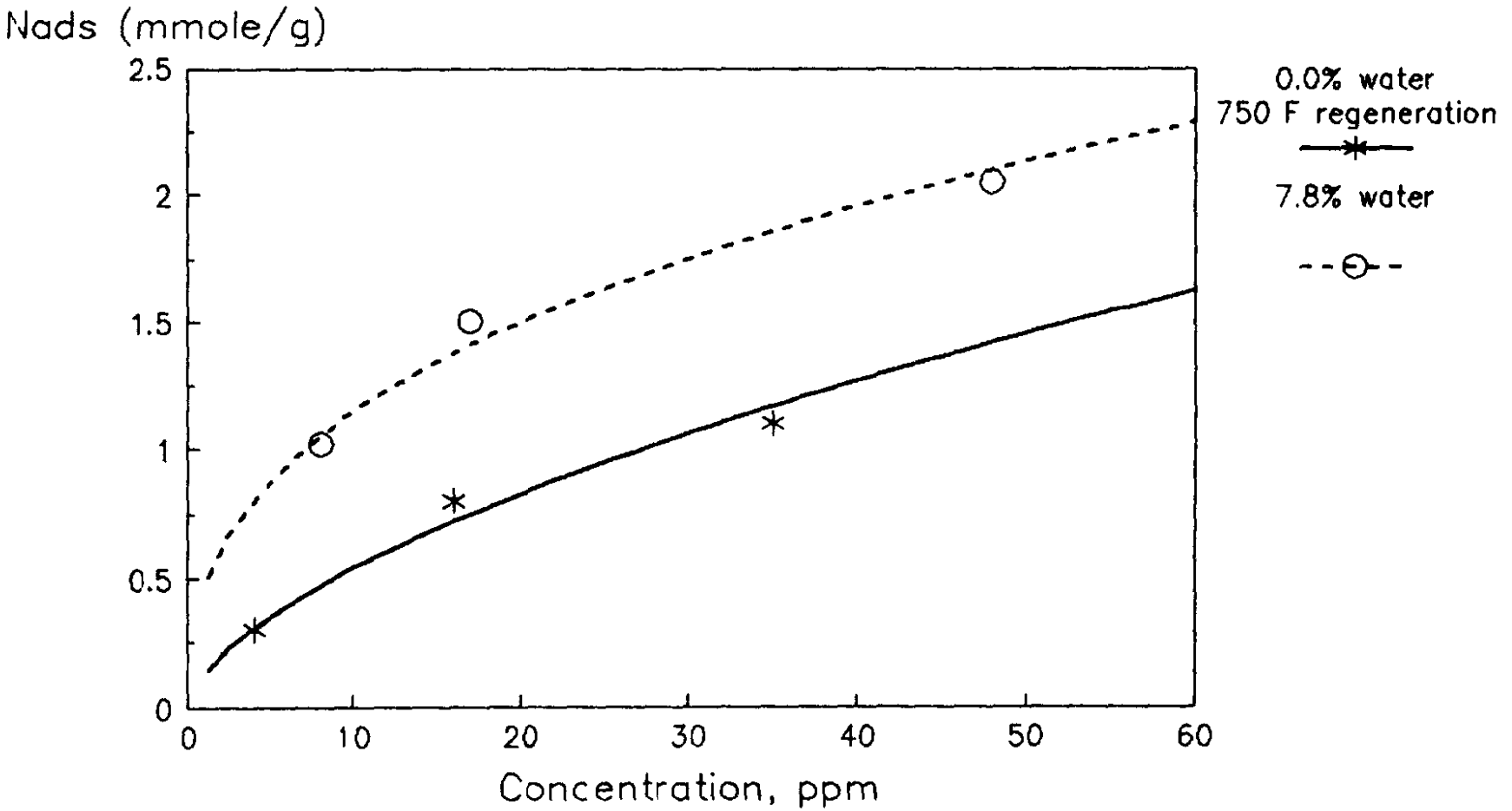

Pilot Unit Design

Estimation of Mass Transfer Zone Lengths

The design of an adsorption system for removal of catalyst poisons from synthesis gas requires an estimation of the mass transfer zone (MTZ) length required for removal of a given impurity. During the dynamic operation of an adsorber bed, there exists both an equilibrium and non-equilibrium zone in the bed. In the equilibrium zone, the adsorbent is in equilibrium with the trace impurity at its inlet concentration. In the non-equilibrium or mass transfer zone, there exists a gradient in gas phase concentration of the impurity which varies from its inlet concentration to essentially zero. The length of the MTZ depends on many variables including the shape of the adsorption isotherm, the rate of mass transfer, the gas flow rate and the adsorbent particle size. Clearly, slow kinetics and unfavorable adsorption equilibrium result in long MTZ lengths which increases adsorber bed size.

The mass transfer coefficients for adsorption of the various trace impurities were estimated from transient uptake curves. The derivation of the kinetic model is given in Appendix B. Once mass transfer coefficients were determined for a given adsorbate/adsorbent system, the mass transfer zone length was estimated by a technique developed by Rosen (5). This technique for estimating MTZ lengths and the kinetic model derived in Appendix B both assume that adsorption isotherms are linear. Linear adsorption isotherms produce MTZ's that spread out as they progress through the adsorption column. Many of the isotherms for catalyst poison removal are not linear, but rather concave to the concentration axis. This type of adsorption isotherm produces MTZs

that sharpen as they proceed through the column. Thus, the linear isotherm assumption, which was made for simplicity, will over predict MTZ lengths.

For a symmetrical mass transfer zone, the length of the zone is given by the equation:

$$MTZ = 2\ [1 - t_i/t_m]\ L$$

where t_i is the time to initial breakthrough, t_m is the time to the midpoint of breakthrough and L is the column length. Therefore, estimation of MTZ lengths requires values for t_i, t_m, and L. The midpoint to breakthrough is calculated from the mass balance on the column using the equation:

$$t_m = L\ \rho_b\ K_H/G$$

where L is the bed length (ft), ρ_b is the bulk density of the adsorbent (lbs/ft^3), K_H is the Henry's law constant for adsorption (lbmoles/lb) and G is the gas flow rate ($lbmoles/ft^2/hr$). After t_m is calculated for a given bed length tehn t_i is calculated from Rosen's solution using the equation:

$$t_i = t_m - 2X\ (tm/K)^{1/2}$$

where K is the mass transfer coefficient in units of reciprocal time and X is a factor that takes into account the initial and final impurity concentration.

Sample Design Calculation

Estimation of column length of H-Y zeolite needed for removal of 5 ppm $Fe(CO)_5$ is given below. The design is based on an adsorption temperature of 75°F, 450 psig total pressure, and a G-rate of 10 lbmoles/ft^2/hr. The Henry's law constant for $Fe(CO)_5$ adsorption under these conditions is estimated from mixed Langmuir considerations to be 15 lbmoles/lb. The experimental value at 75°F and 90 psig carrier is 30 lbmoles/lb (0.15 mlbmoles/lb/5 ppm). The mass transfer coefficient determined from lab data is 46.3 hr^{-1}. The value of k determined from Appendix B is in units of lbmole/lb/min. To get k in units of reciprocal time, division by the Henry's law constant is necessary. Assuming the inlet $Fe(CO)_5$ concentration is 5 ppm and the outlet is 0.01 ppm, the value of X is 2.0. The bulk density of H-Y zeolite is 40 lbs/ft^3. MTZ lengths calculated for various bed lengths are given below:

L (ft)	t_m (hr)	t_i (hr)	MTZ (ft)
1.0	60.0	55.4	0.15
0.5	30.0	26.8	0.11
0.25	15.0	12.7	0.08

These calculations indicate that a column length of 0.5 ft will demonstrate initial breakthrough of $Fe(CO)_5$ after 27 hours on-stream. Similar calculations were done for $Ni(CO)_4$, COS, H_2S, and HCl removal. The value needed for these calculations are given in the following table:

Adsorbent	Poison	(lbmole/lb) K_H	(hr^{-1}) k	(lbs/ft^3) ρ_b	X
BPL	$Ni(CO)_4$	24	5.6	30	1.7
FCA	COS	3.8	2.8	30	2.1
BASF S3-85	H_2S	400	0.10	80	2.0
BASF S3-85	HCl	1000	0.20	80	2.5

Using these values, the following pilot unit design was achieved:

Bed 1: BASF S3-85 for adsorption of H_2S and HCl in a throw-away system. Calculations suggest that under the conditions specified above, a 0.5 ft bed of BASF S3-85 should last about 50 days with inlet concentrations of 20 and 5 ppm for HCl and H_2S, respectively.

Bed 2: H-Y zeolite for removal of $Fe(CO)_5$. A 0.5 ft bed is estimated to last 27 hours on-stream as indicated previously. Thermal regeneration in N_2 at 250°F is required for reactivation.

Bed 3: BPL carbon for removal of $Ni(CO)_4$. A 0.5 ft bed is estimated to last 29 hours on-stream. Thermal regeneration in N_2 at 250°F is required for reactivation. These calculations assume an inlet concentration of 1 ppm and an outlet of 0.01 ppm.

Bed 4: FCA carbon for removal of COS. A 3.5 ft bed is estimated to last 25 hours on-stream. Thermal regeneration in N_2 at 500°F is required for reactivation. These calculations assume an inlet concentration of 10 ppm and an outlet of 0.01 ppm.

REFERENCES

1. The LPMEOH Process - An Efficient Route to Methanol from Coal, G. W. Roberts, N. K. Dicciani, and J. Klosek, presented at the conference on Coal Gasification and Synthetic Fuels for Power Generation, April 1985.

2. T. C. Golden, Front End Clean-Up of Landfill Gas - Adsorption of Trace Compounds from CO_2, RRRS No.: APCI/PSG-85/008.

3. Nagy, J. B., Van Eunoo, M. and Derovane, E. G., Journal of Catalysis, 58, 230-237 (1979).

4. Dwyer, D. J. and Somorjai, G. A., Journal of Catalysis, 52, 291 (1978).

5. Rosen, J. B., Industrial and Engineering Chemistry, 46(8), 1590 (1954).

Appendix A

ANALYSIS REPORT

TO: P. Stepanoff DEPT.: PSG Research, Iron Run

FROM: J. H. Phillips, K. C. Tewari DEPT.: CRSD-A, R&D 3/x. 5673,4791

DATE: 28 October 1986 Problem Solving Laboratory

SUBJECT: GC/ECD Analysis of Iron and Nickel Carbonyls

Sample No.: SG27010

---

cc: J. H. Frost; F. A. Lucrezi; G. J. Mantell; P. Rao; T. L. Slager

SUMMARY: A packed column gas chromatograph equipped with an electron capture dete tor (GC/ECD) has been set up to measure nickel tetracarbonyl ($Ni(CO)_4$) and iron pentacarbonyl ($Fe(CO)_5$) in syngas. A dynamic gas diluter was utilized for calibration of the instrument and the determination of method linearity. The GC/ECD and dynamic diluter were found to be linear over five orders of magnitude. The detection limit and quantitation limit for $Ni(CO)_4$ were 0.03 ppb and 1.0 ppb, respectively. The detection limit and quantitation limit for $Fe(CO)_5$ were 0.15 ppb and 0.27 ppb, respectively. The concentration of $Ni(CO)_4$ and $Fe(CO)_5$ in syngas cylinder SG27010 as measured by GC/ECD was in good agreement with the traditional method of analysis.

PROBLEM DEFINITION/SAMPLE DESCRIPTION: Both $Fe(CO)_5$ and $Ni(CO)_4$ are known to be catalyst poisons at trace levels in the liquid methanol process. The traditiona method of $Fe(CO)_5$ and $Ni(CO)_4$ analysis consists of wet scrubbing followed by atomic absorption analysis for iron and nickel. The Process Gas Group requested ar analytical technique with a faster turnaround time to allow a more rapid response to catalyst poisoning. Tests were also scheduled in which various materials would be evaluated for their ability to remove metal carbonyls from the syngas. Due to the large volume of gas required for the traditional method, a new technique which used a smaller sample size would be preferred. The syngas consists of approximatel 37% H_2, 36% CO_2, 20% CO, and 0.9% N_2.

ANALYTICAL PROCEDURES: The 5890 GC/ECD and 3393A integrator were purchased from Hewlett-Packard. A slight modification was made to the gas sampling valve system according to Figure 1. The column was silanized prior to packing and conditioned overnight at 100°C before use. The GC/ECD operating conditions are listed in Table 1, and typical chromatograms can be found in Figure 2. The dynamic gas diluter utilized two Tylan GC260 mass flow controllers and was designed and assembled at APCI. A schematic diagram of the dynamic diluter can be found in Figure 3.

Request No.: None
Charge No.: 87-7-1557.71
Notebook No.: 9189-12
Method No.: 274
Phone Date: 10/27/86
Sample Receipt Date: 10/6/86

lkw:4022w

RESULTS AND DISCUSSION: Once the instrumental conditions described in Table 1 wer set up, a standard cylinder containing 22 ppm $Fe(CO)_5$ and 8 ppm $Ni(CO)_4$ was connected to the gas sampling loop. Since both carbonyls eluted much more rapidly than expected, a liquid standard of 6 ppm $Fe(CO)_5$ was injected to confirm the retention time of that component. Next, the dynamic gas diluter was utilized to produce accurate, real time, low level carbonyl standards for a calibration curve. In this work, the standard cylinder was diluted with nitrogen, and the dynamic gas diluter outlet was connected directly to the gas sampling loop. The data obtained from this procedure is listed in Table 2, and log-log plots of the standard curves can be found in Figures 4 and 5. Both $Fe(CO)_5$ and $Ni(CO)_4$ calibration curves were linear down to 1.0 ppb. Below 1.0 ppb, the quantitation of $Ni(CO)_4$ was difficult since it eluted on the tail of an impurity in the nitrogen. In the syngas matrix, this problem is not expected, and lower detection and quantitation limits should be achievable for $Ni(CO)_4$.

To confirm the accuracy of the GC/ECD technique, a standard cylinder and a syngas cylinder (SG27010) were analyzed simultaneously by GC/ECD and the traditional method. First the syngas cylinder was analyzed. During the 30 minute scrub time, seven GC/ECD measurements were taken. Next, the standard cylinder was placed in line. During the 40 minute scrubbing time, the standard cylinder was analyzed by GC/ECD to arrive at standard response factors for the iron and nickel carbonyl peaks. For this work, the standard cylinder was connected to the dynamic diluter prior to the GC/ECD. In this way, the external calibration standard could be dynamically diluted until the area counts of the external standard approximated the area counts in the sample. The $Ni(CO)_4$ area counts stabilized almost immediately, however, the $Fe(CO)_5$ area counts were extremely low until about 30 minutes into the analysis. Since the traditional method found no significant variation from previous measurements, we are assuming that $Fe(CO)_5$ requires a significant period of time to equilibrate in the dynamic diluter. After the levels of $Fe(CO)_5$ and $Ni(CO)_4$ in the standard cylinder were determined by the traditional method, a response factor for each analyte was calculated. By applying these response factor to the average area counts in the syngas, $Fe(CO)_5$ and $Ni(CO)_4$ concentrations were calculated (Table 3).

The GC/ECD technique is able to accurately and precisely measure less than 1.0 ppb concentrations of $Fe(CO)_5$ and/or $Ni(CO)_4$ in syngas. The sample volume required for the 1.0 ppb quantitation limit is 1.0 ml, and the analysis time is under 3.0 minutes. Personnel from CRSD-Analytical will be available to help PSG researchers utilize the GC/ECD instrument for future measurements. A CRSD-Analytical method, entitled "Analysis of Trace Levels of $Fe(CO)_5$ and $Ni(CO)_4$ in Syngas", is currently being written.

John H. Phillips
J. H. Phillips

K. C. Tewari
K. C. Tewari

lkw:4022w
Attachments

Table 1

GC/ECD Operating Conditions

Column:	6' x 2 mm i.d. (.25" o.d.) glass
Packing:	10% squalane on 100/120 mesh chromosorb W (H/P)
Carrier:	5% methane in Argon at 60 ml/min.
Oven:	31°C, isothermal
Injector:	31°C, 1 ml gas sampling loop
Detector:	31°C, Ni^{63} Electron Capture
Integrator:	3393A Hewlett-Packard

Table 2

Calibration Standards for $Ni(CO)_4$ and $Fe(CO)_5$

$Ni(CO)_4$			$Fe(CO)_5$		
ppb	Counts	% rsd	ppb	Counts	% rsd
8,000.	2.044ee7	3.2	22,000.	1.196ee8	2.8
800.	2.622ee6	1.8	2,200.	1.926ee7	4.8
63.	3.778ee5	13.0	540.	4.033ee6	3.1
6.3	7.561ee4	4.7	54.	2.268ee5	3.9
1.26	1.809ee4	1.9	10.8	4.052ee4	4.1
0.63	1.141ee4	4.4	5.4	1.866ee4	2.0
0.315	8.789ee3	4.6	2.7	1.089ee4	2.2
0.063	3.417ee3	5.3	0.54	2.563ee3	9.0
0.0315	2.748ee3	3.2	0.27	1.330ee3	16.0
			0.216	2.370ee2	28.1
			0.162	2.020ee2	31.0

Table 3

Calibration Results GC/ECD vs. Traditional Method

Standard Cylinder Calibration and GC/ECD Response Factors

Ni(CO)4	15.0 ppm by A.A.	4,730,000 cts/ppm	1.7 %rsd (n=3)
Fe(CO)5	9.9 ppm by A.A.	8,230,000 cts/ppm	3.0 %rsd (n=3)

Syngas Sample (SG27010) Analysis by A.A. and GC/ECD

Ni(CO)4	0.056 ppm by A.A.	0.063	2.0 %rsd (n=7) by GC/ECD
Fe(CO)5	0.47 ppm by A.A.	0.54	3.5 %rsd (n=7) by GC/ECD

4022w

Position 1

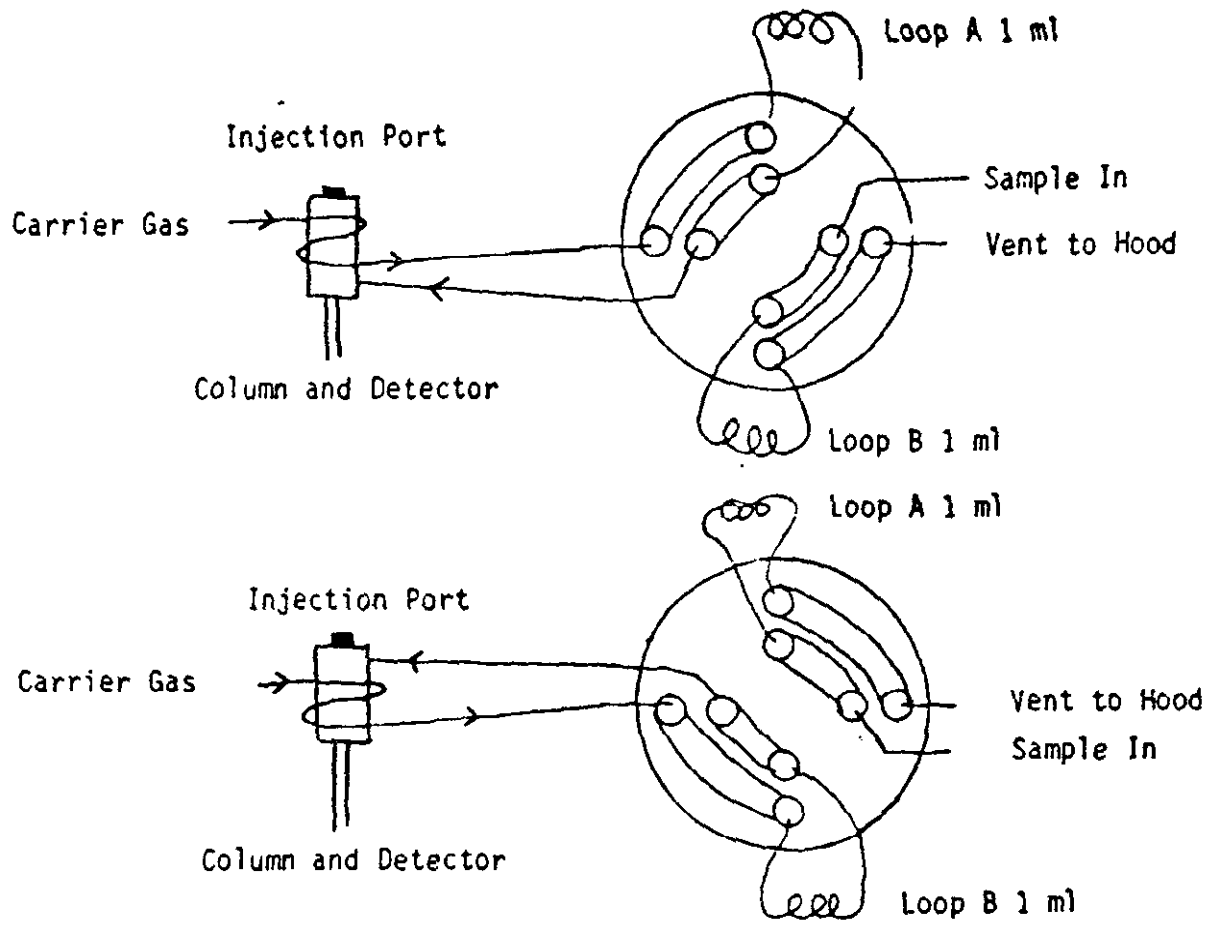

Position 2

Figure 1

Eight Port Sample Valve Configuration

Figure 2

GC/ECD Chromatograms

63 ppb $Ni(CO)_4$

540 ppb $Fe(CO)_5$

In Nitrogen

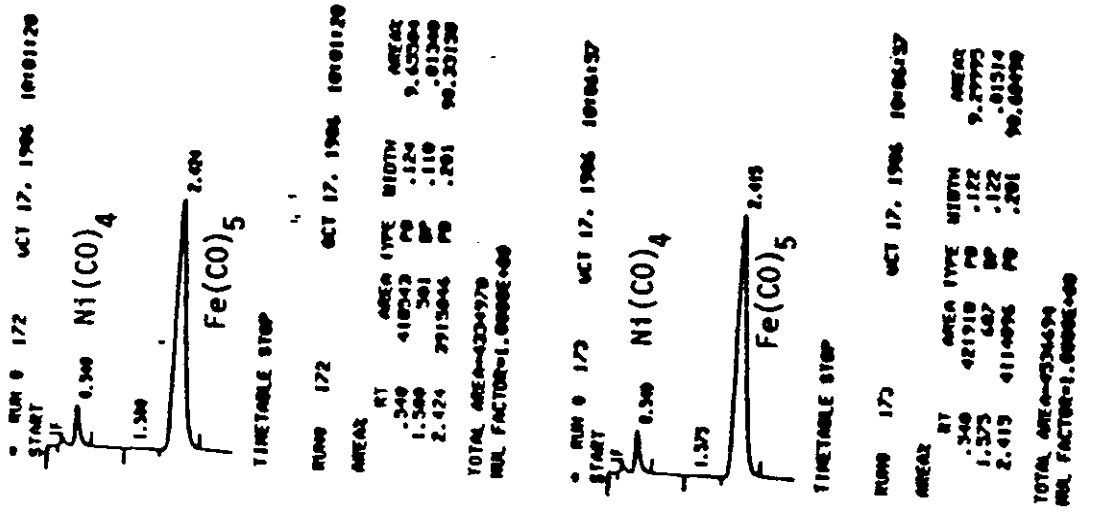

6.3 ppb $Ni(CO)_4$

54 ppb $Fe(CO)_5$

In Nitrogen

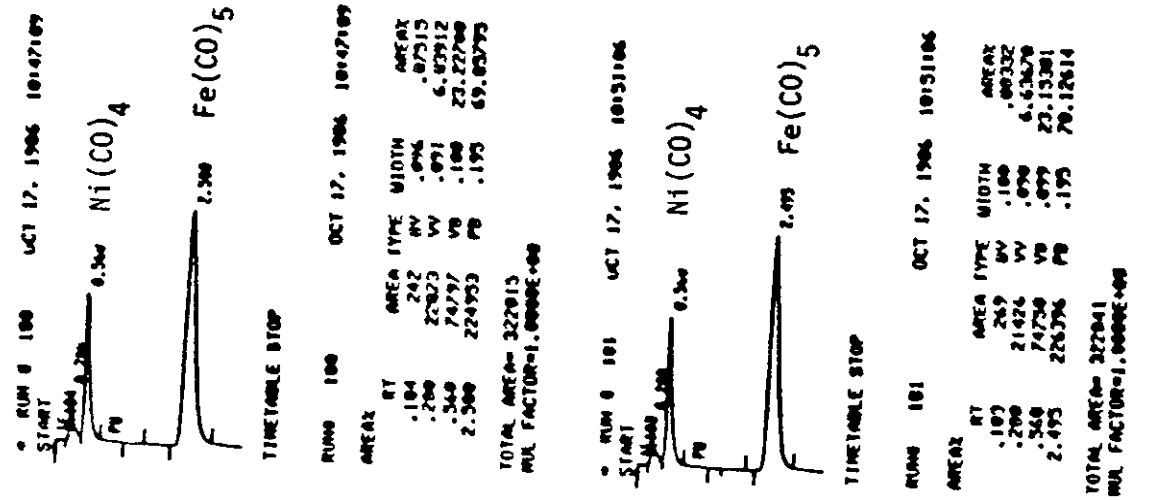

0.03 ppb $Ni(CO)_4$

0.27 ppb $Fe(CO)_5$

In Nitrogen

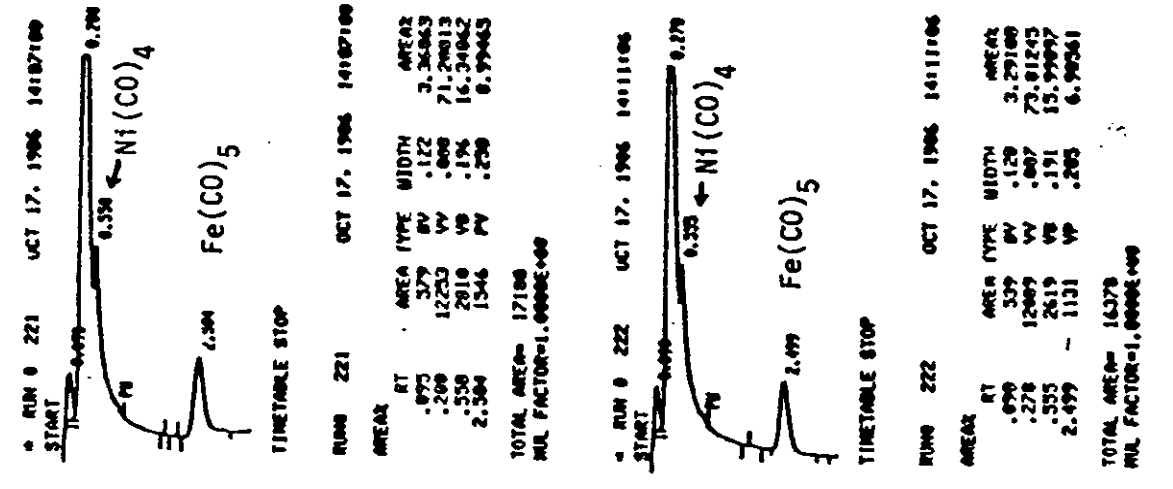

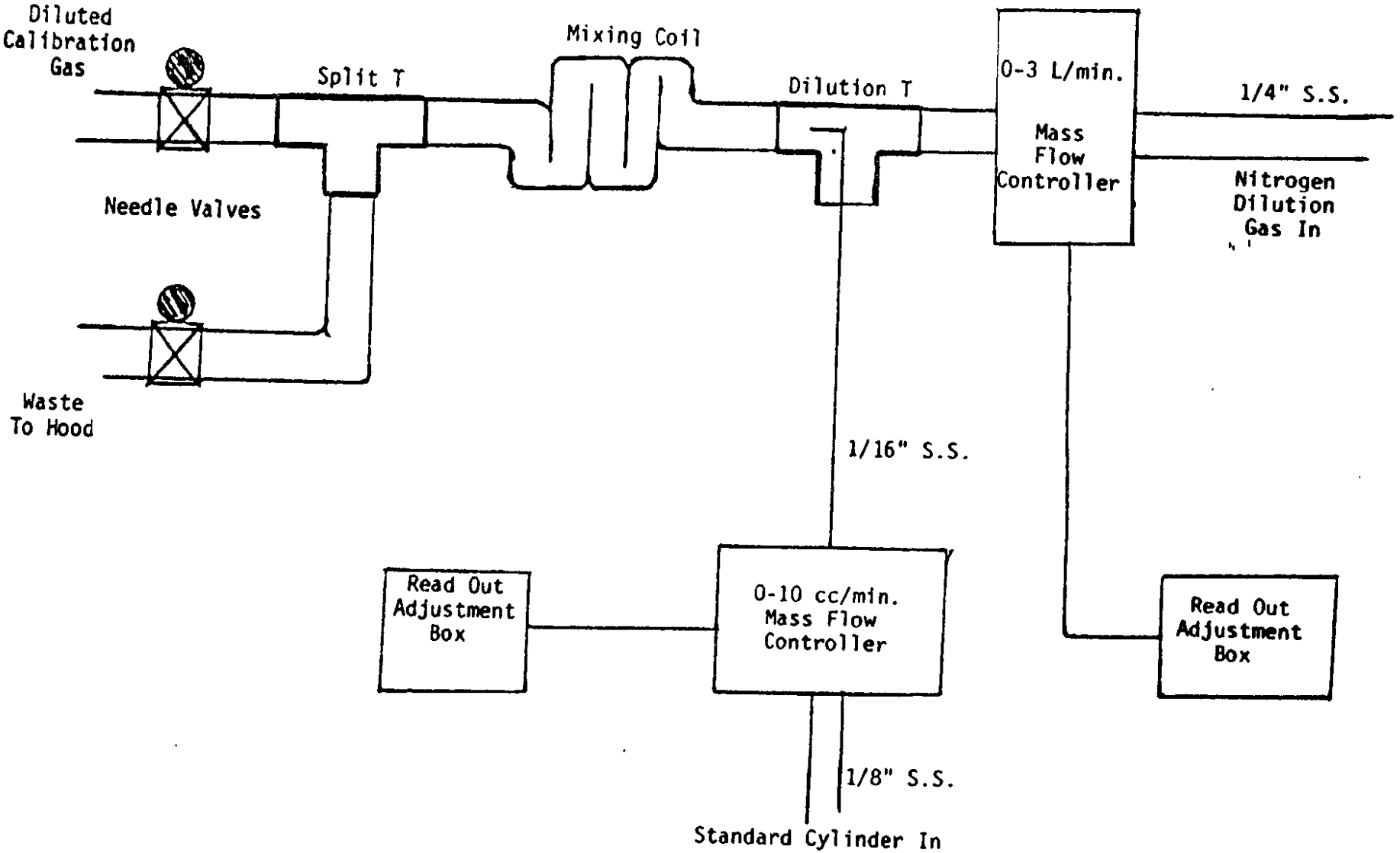

Figure 3

Dynamic Gas Diluter Schematic Diagram

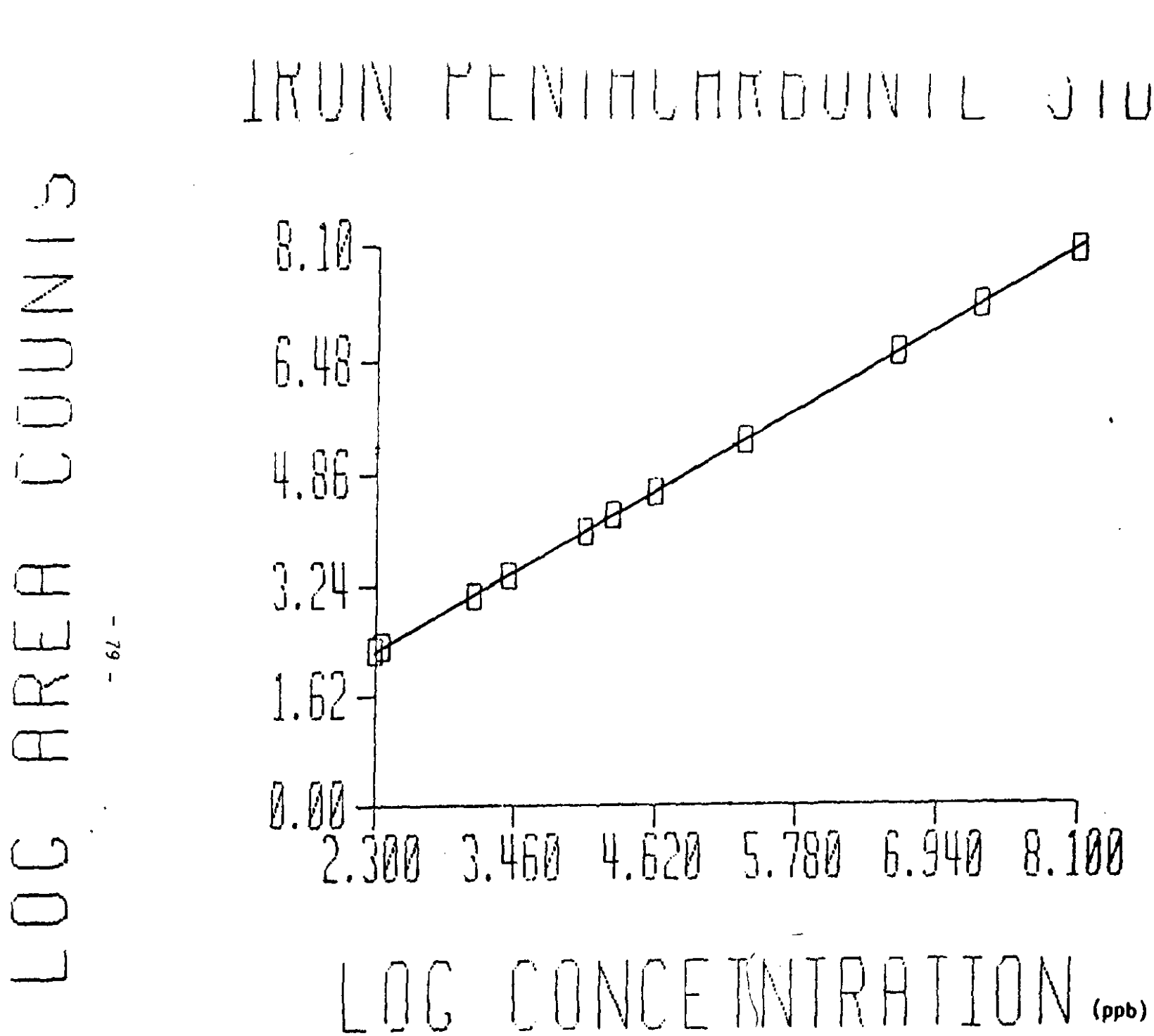
IRON PENICLLAMINE STD.
LOG AREA COUNTS
8.10
6.48
4.86
3.24
1.62
0.00
2.300
3.460
4.620
5.780
6.940
8.100
LOG CONCENTRATION (ppb)

Figure 5

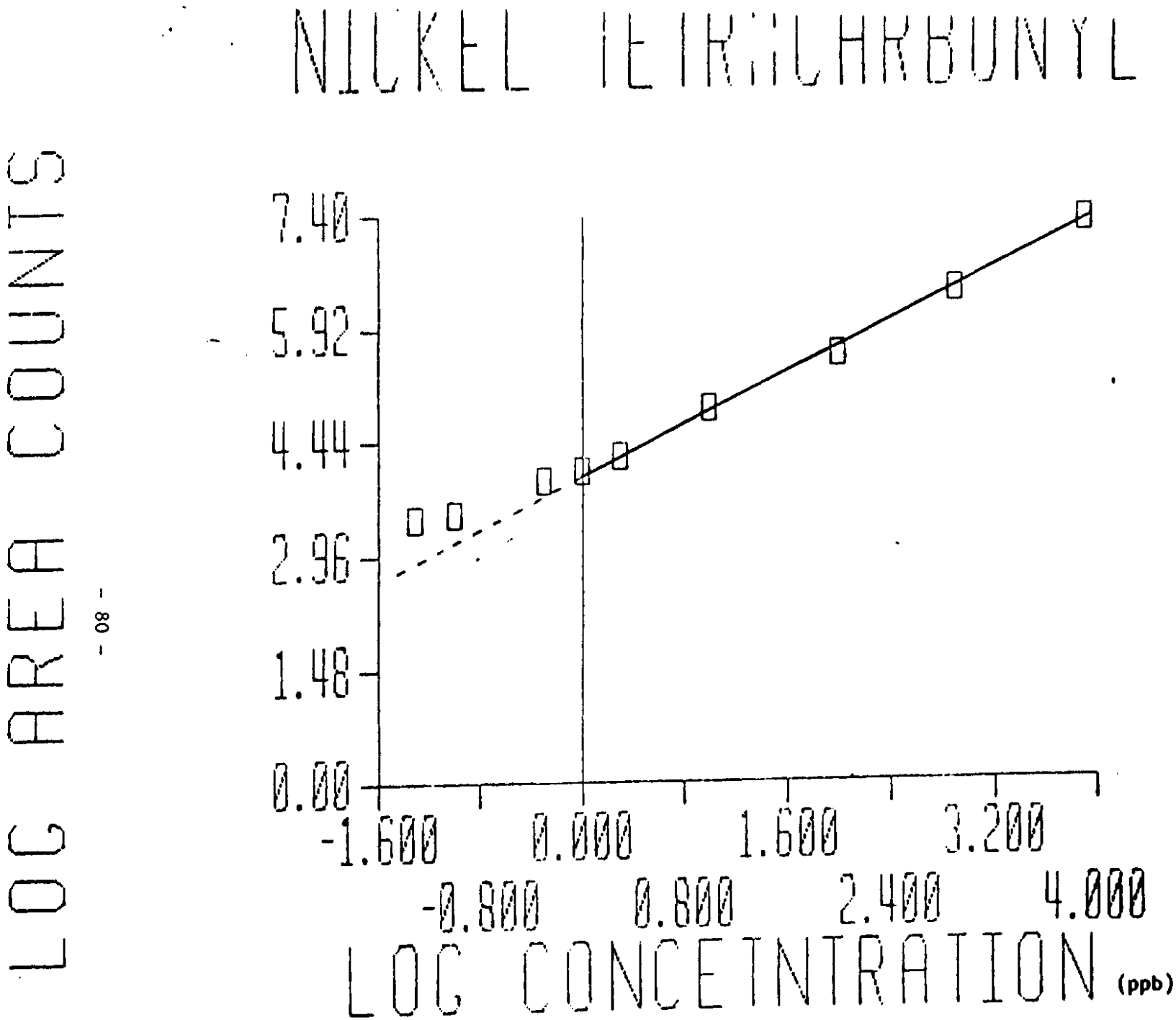
NICKEL TETRACARBONYL
LOG AREA COUNTS
7.40
5.92
4.44
2.96
1.48
0.00
-1.600
0.000
1.600
3.200
-0.800
0.800
2.400
4.000
LOG CONCETNTRATION (ppb)

Figure 4

Figure 1. Chromatogram Showing the Separation of 1.8 ppmv H_2S and 1.6 ppmv COS from 30% H_2, 20% N_2, 10% CO, and 40% CO_2

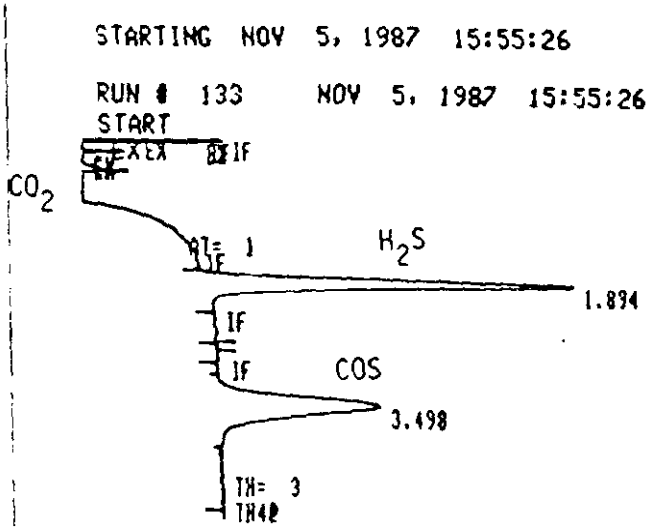

RUN# 133 NOV 5, 1987 15:55:26

SAMPLE# 170

AREA%

RT	AREA	TYPE	WIDTH	AREA%
1.894	91262	I BB	.139	52.74589
3.498	81760	PV	.288	47.25411

TOTAL AREA= 173022
MUL FACTOR=1.0000E+00

APPENDIX B

Derivation of Kinetic Model

At the start of kinetic measurements (t = o), there is a known amount of impurity in the gas phase, y_o, and a known amount of impurity adsorbed on the carbon, n_i. As the kinetic experiment starts (t > o), the gas phase impurity is exposed to the adsorbent and during adsorption the gas phase concentration, y, decreases as a function of time.

Mass Balance at Any Time

$$W\, dn/dt = \frac{PV}{RT}\, dy/dt$$

where W = adsorbent weight

n = number of moles in gas phase

t = time

P = total pressure, constant

V = total void volume, constant

T = temperature, constant

y = impurity concentration

Let a = PV/WRT, then

$$\frac{dn}{dt} = a\,\frac{dy}{dt}$$

Integrating yields:

$$\int_{n_i}^{n} dn = a \int_{y_o}^{y} dy$$

$$(n-n_i) = a\,(y-y_o) \qquad \text{or} \qquad (1)$$

$$n = n_i + a\,(y-y_o)$$

Rate of Mass Transfer

The rate of mass transfer is given by:

$$\frac{\partial n}{\partial t} = k(y - \bar{y}) \qquad (2)$$

where k is the mass transfer coefficient in units gmole/gm/sec.

If the adsorption isotherm is linear, then it can be described by:

$$n = K\,\bar{y} \qquad (3)$$

Combining equations 2 and 3 yields:

$$\frac{\partial n}{\partial t} = k\left(y - \frac{n}{K}\right) \qquad (4)$$

Combining equations 1 and 4 yields:

$$a\frac{\partial y}{\partial t} = k\left[y - \frac{n_i + a(y - y_o)}{K}\right]$$

$$= k\left[y\,(1-a/k) - \left(\frac{n_i - ay_o}{K}\right)\right]$$

Let $b = 1 - a/k$

$$c = \frac{n_i - ay_o}{K}$$

Substitution leaves:

$$a\frac{\partial y}{\partial t} = k\,[by - c]$$

Integrating:

$$\int_{y_o}^{y} \frac{dy}{(by-c)} = \frac{k}{a}\int_{o}^{t} dt$$

$$\left.\frac{1}{b}\ln(by - c)\right]_{y_o}^{y} = \frac{k}{a}\,t$$

Evaluating leaves:

$$\ln \frac{by - c}{by_o - c} = \frac{b}{a} kt \qquad (5)$$

Substituting values for b and c leave:

$$by_o - c = y_o - n_i/k$$

and

$$by - c = y\left(1 - \frac{a}{k}\right) - \frac{1}{k}\left(n_i - ay_o\right)$$

Substituting these values into equation 5 yields:

$$\ln \frac{y(1-a/k) - \frac{(n_i - ay_o)}{K}}{y_o - n_i/k} = \left(\frac{k-a}{ak}\right) kt$$

or

$$\ln \frac{y(1-a/k) - \frac{(n_i - ay_o)}{K}}{y_o - n_i/k} = \exp\left(\frac{k-a}{ak}\right) kt$$

Thus by plotting the left hand side of the above equation vs. $t\left(\frac{k-a}{ak}\right)$ yields a straight line with a slope of k in units of gmole/gm/sec.